JBIC Journal of Biological Inorganic Chemistry (2024) 29:455–475
https://doi.org/10.1007/s00775-024-02058-w

ORIGINAL PAPER

Iron mobilization from intact ferritin: effect of differential redox activity of quinone derivatives with NADH/O_2 and in situ-generated ROS

Narmada Behera[1] · Gargee Bhattacharyya[1] · Satyabrat Behera[1] · Rabindra K. Behera[1]

Received: 17 January 2024 / Accepted: 10 April 2024 / Published online: 23 May 2024

Abstract
Ferritins are multimeric nanocage proteins that sequester/concentrate excess of free iron and catalytically synthesize a hydrated ferric oxyhydroxide bio-mineral. Besides functioning as the primary intracellular iron storehouses, these supramolecular assemblies also oversee the controlled release of iron to meet physiologic demands. By virtue of the reducing nature of the cytosol, reductive dissolution of ferritin-iron bio-mineral by physiologic reducing agents might be a probable pathway operating in vivo. Herein, to explore this reductive iron-release pathway, a series of quinone analogs differing in size, position/nature of substituents and redox potentials were employed to relay electrons from physiologic reducing agent, NADH, to the ferritin core. Quinones are well known natural electron/proton mediators capable of facilitating both 1/2 electron transfer processes and have been implicated in iron/nutrient acquisition in plants and energy transduction. Our findings on the structure–reactivity of quinone mediators highlight that iron release from ferritin is dictated by electron-relay capability (dependent on $E_{1/2}$ values) of quinones, their molecular structure (i.e., the presence of iron-chelation sites and the propensity for H-bonding) and the type/amount of reactive oxygen species (ROS) they generate in situ. Juglone/Plumbagin released maximum iron due to their intermediate $E_{1/2}$ values, presence of iron chelation sites, the ability to inhibit in situ generation of H_2O_2 and form intramolecular H-bonding (possibly promotes semiquinone formation). This study may strengthen our understanding of the ferritin-iron-release process and their significance in bioenergetics/O_2-based cellular metabolism/toxicity while providing insights on microbial/plant iron acquisition and the dynamic host–pathogen interactions.

Dedicated to Prof. Shyamalava Mazumdar (Senior Professor – Tata Institute of Fundamental Research, Mumbai, India).

Extended author information available on the last page of the article

Graphical Abstract

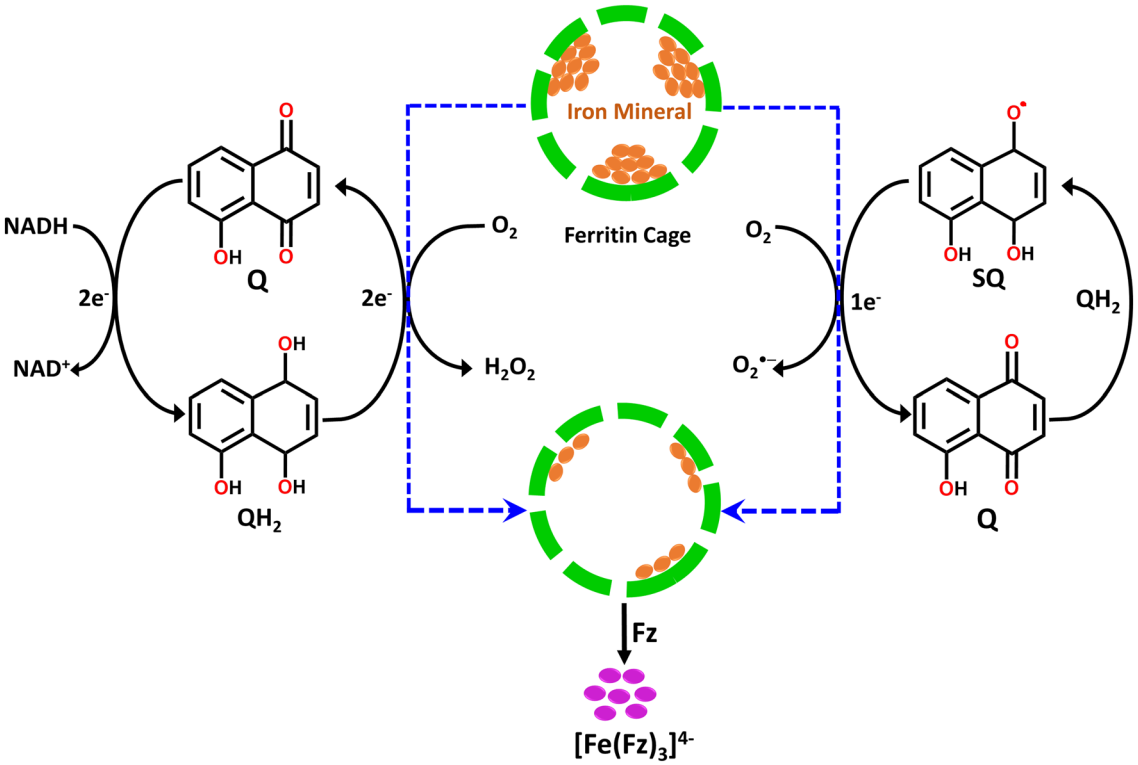

Keywords Ferritin · Protein-cage · Iron release · Electron transfer · Mediator · Quinones

Abbreviations

NADH	*β*-Nicotinamide adenine dinucleotide
BQ	Benzoquinone
HQ	Hydroquinone
NQ	Naphthoquinone
MN	Menadione
MNS	Menadione sulphonate
LW	Lawsone
JG	Juglone
PM	Plumbagin
FL	Follin
AQS	Anthraquinone sulphonate
ET	Electron transfer
F_{ox}	Ferroxidase center
Mtb	*Mycobacterium tuberculosis*
BfrB	Bacterioferritin B
MOPS	3-(N-morpholino) propane sulfonic acid
$E_{1/2}$	Mid-point potential
CV	Cyclic voltammetry
SWV	Square wave voltammetry
DPV	Differential pulse voltammetry
ROS	Reactive oxygen species
Q	Quinone (oxidized form)
Q_{ox}	Oxidized quinone
SQ	Semi-quinone (one electron reduced form)
QH_2	Quinol (two electron reduced form)
Fz	Ferrozine
NBT	Nitro blue tetrazolium salt
DMSO	Dimethyl sulfoxide
HRP	Horse radish peroxidase
SOD	Superoxide dismutase
pI	Isoelectric point

Introduction

Iron, an essential micronutrient, is crucial to almost all living organisms: bacteria, plants, animals, and humans. As an active/vital component of numerous proteins and enzymes, iron is closely tied with a wide range of crucial biologic processes (O_2 transport, ATP synthesis, N_2 fixation, DNA synthesis/repair/replication, etc.) while being metabolically

shuttled between its oxidized (Fe^{3+}) and reduced (Fe^{2+}) forms [1, 2]. The redox activity of iron is finely tuned in nature by manipulation of its primary/secondary coordination sphere for its participation in electron transfer (ET) or catalytic transformations [2, 3]. Although the redox cycling of iron is a critical aspect for its biologic preference/selection, it is often associated with the generation of toxic free radicals via Fe^{2+}- based Fenton reaction [4, 5]. Furthermore, Fe^{3+} has low solubility (~ 10^{-18} M) under circumneutral environments that limits its bioavailability, despite being a relatively abundant element on the Earth's crust [6, 7]. Thus, iron uptake, storage, and utilization by organisms require stringent control and systematic regulation to maintain its optimum physiologic levels [1, 8].

To address this dual/dichromatic nature of iron in physiologic systems (toxicity versus essentiality), organisms encode a multimeric nanocage protein 'ferritin' that sequesters, detoxifies, and acts as cellular storehouses of iron [8–11]. Ferritins scavenge Fe^{2+} and catalytically oxidize it in the presence of O_2/H_2O_2 to concentrate iron as a ferric oxyhydroxide bio-mineral ($nFe_2O_3.xH_2O$) in its central nanocavity [11–15]. Structurally, ferritins are made up of 24 polypeptide subunits that spontaneously self-assemble into a spherical nanocage structure with a hollow chamber (~ 12 nm: external shell diameter, ~ 8 nm: inner core diameter) [16–19]. The internal nanocavity is connected to the external (cytoplasmic) environment by symmetric/asymmetric pores/channels [20]. Facilitated diffusion of Fe^{2+} ions through these hydrophilic channels toward the catalytic di-iron ferroxidase centers, are electrostatically guided by strategically placed amino acid residues [12, 21–24]. Variations in the composition and position of amino acids at/in the vicinity of the channels/ferroxidase centers/internal surface of the protein cage dictate the local electrostatics, iron uptake ability, kinetics/mechanism of biomineralization, nature/stability of the ferric oxyhydroxide core and possibly the reverse process (iron-mineral core reduction and its dissolution followed by subsequent exit of iron from ferritin) [24–29].

Besides mitigating the unwanted outflow of Fe^{2+} into the cytosol, ferritins are also responsible for the controlled release of iron for cellular/metabolic activities [30, 31]. Although iron uptake and bio-mineralization processes are relatively well explored in the ferritin family, the mechanism/routes of iron dissolution/mobilization remain elusive [32–34]. Further, this release of iron from ferritin is intricately linked to iron acquisition/utilization by pathogens [35–37]. As a part of the immune response, the host restricts iron availability to pathogens by sequestering it within ferritin (via upregulation of ferritin synthesis), thereby limiting the essential nutrient for microbial growth [35, 38]. Pathogens, in turn, have evolved sophisticated mechanisms (siderophore-based chelation, proteolytic degradation and reductive pathway) to acquire iron from the host resulting in a long standing host–pathogen battle for iron [39, 40]. Owing to its versatile redox properties, the role of iron in microorganisms is well beyond mere nutritional requirements. In some microorganisms, Fe^{3+} mineral can function as a terminal electron acceptor under limited supply of oxygen to meet the energy requirements for fueling the proton pump (iron-respiration) [41, 42]. Pathogens synthesize both heme and non-heme binding ferritins for their iron metabolism and growth as well as to protect themselves from oxidative stress. Understanding the dynamic host–pathogen interaction may be beneficial for developing strategies to disrupt pathogen iron acquisition/storage/mobilization/utilization and strengthen the host's defense against infections [37, 39].

The mechanisms of in vivo iron release are yet to be concretely established, though several possible theories have been put forward, which includes: NCOA4-mediated ferritinophagy [43], selective gating of ferritin pores [44], direct Fe^{3+} chelation and reductive pathway [34, 45–47]. In addition to experimental research, molecular dynamic simulations have been adapted to understand the iron release from ferritin in acidic environment such as endosomes and lysosomes [33, 48]. Proteolytic/proteosomic degradation is one of the ferritin iron-release pathways established in the last decade [43, 49, 50], where the ferritin protein cage undergoes degradation by proteolytic enzymes, leading to disruption of protein coat and spillage of iron mineral. On the contrary, the reductive iron-release pathway involves bio-mineral dissolution and mobilization from intact ferritins driven by reducing agents/electron mediators/chelators and could be considered a reasonable pathway/possibility in vivo, due to the reducing nature of the cytosol [51]. The existence of reductive pathway of iron mobilization from ferritin/bacterioferritin is reported in pathogens like *Pseudomonas aeruginosa* (*P. aeruginosa*) [52], *Escherichia coli* (*E. coli*) [53] and *Mycobacterium tuberculosis* (*Mtb*) [36]. In these pathogens, redox active heme facilitates reductive iron release from heme-binding ferritin (bacterioferritin, Bfr), possibly acting as an intrinsic ET mediator [36]. Moreover, in case of *P. aeruginosa*, reductive iron release from Bfr is facilitated by binding of a [2Fe-2S] based ET protein, Bfd (an electron shuttle) onto its surface (forming a Bfr-Bfd complex) [52]. However, for the intracellular pathogen, *Mtb*, the reducing agent and its redox partner/mediator participating in the iron release from its non-heme binding ferritin (BfrB) is not well defined [54]. Physiologic reducing agent like NADH, a 2 e^- donor, is not efficient for this purpose, when used alone [55]. Therefore, finding a suitable electron shuttle is essential to carry out long range ET, across protein shell to reduce the encapsulated iron-mineral core.

Quinones are versatile and ubiquitous redox cofactors (participates both in 1 and 2 e^- transfer), which play a pivotal role in facilitating important biologic processes such as photosynthesis (photophosphorylation), aerobic/anaerobic

respiration (oxidative phosphorylation, where O_2 or iron act as terminal electron acceptor), and NAD(P)H dependent enzymatic reactions [41, 42, 56]. Their electron shuttling enables them to maintain the transmembrane proton gradients required for ATP synthesis. Quinones have been extensively used for detection and sensing of physiologic reducing agents [57]. Some quinones such as plumbagin and juglone participate in iron acquisition in plants [58]. The presence of suitable functional groups (Fig. 1), keto and hydroxyl, in quinone derivatives, make them potential candidates for ET mediator/iron chelator. Due to their redox ability and tunable nature, quinones are the key components in technologies such as dye-sensitized solar cells, microbial fuel cells and catalysis [59, 60]. Moreover, quinones may be generated in ferritin by oxidation of tyrosine residues (by Fenton reaction of ferritin substrates: Fe^{2+} and H_2O_2) and can influence the iron oxidation/mineralization and mineral reduction/release by shuttling protons and electrons [61].

Herein, we explore the reductive approach of iron mobilization from non-heme binding *Mtb* ferritins using physiologic reducing agent, NADH, in conjugation with quinone-based electron-relay molecules, which can potentially shuttle electrons between NADH (electron source) and the iron-mineral core (sink). The current report

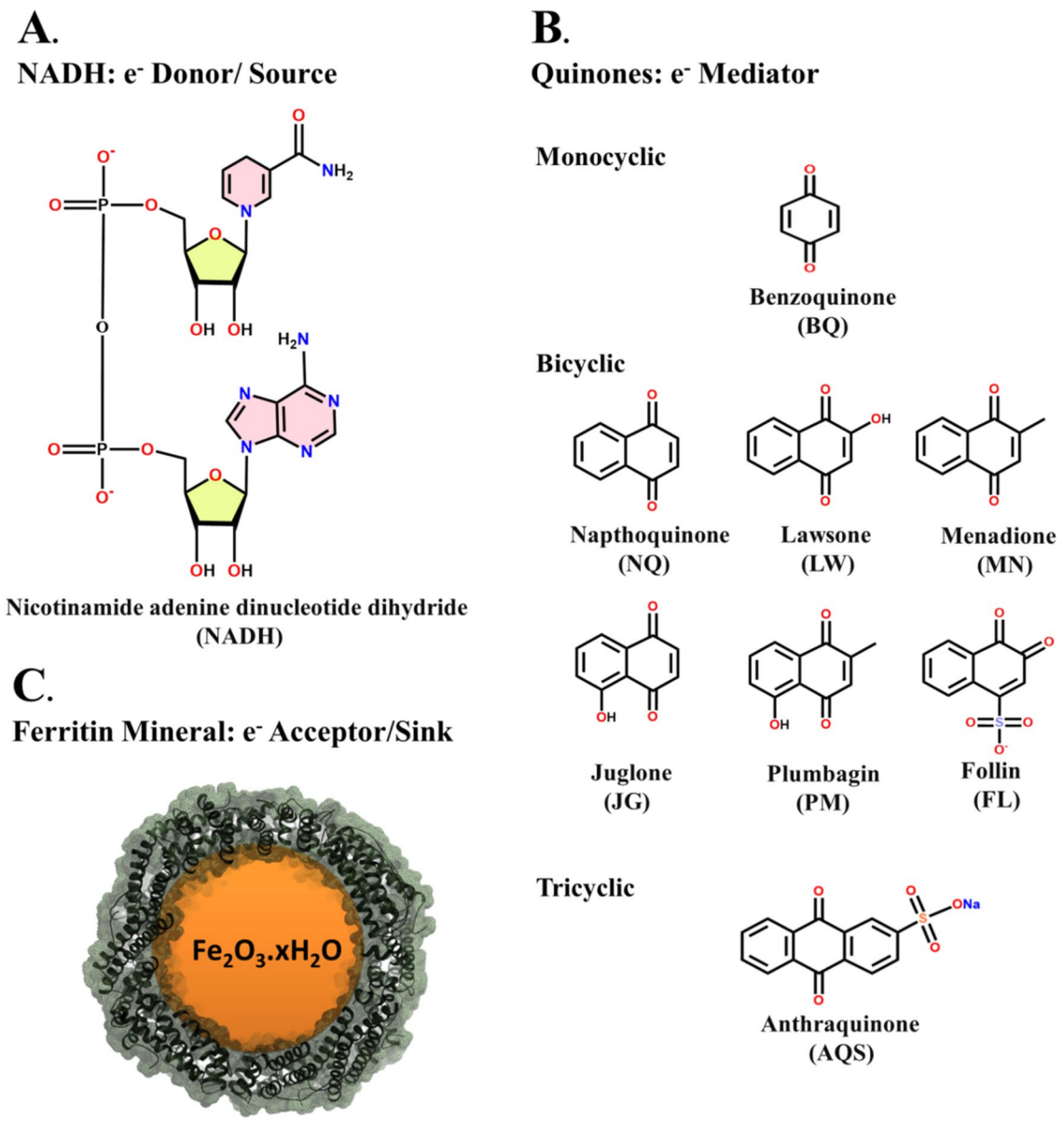

Fig. 1 Structure of physiologic reducing agent NADH (e^- donor: **A**), quinone analogs (e^- mediator: **B**) and ferritin protein-caged iron mineral (e^- acceptor: **C**) used in this report to investigate the differential reactivities facilitating reductive iron mobilization

utilizes a set of quinone derivatives differing in size, substituent nature/positions, metal-ion chelating ability and mid-point potential values to study their reactivity with NADH/O_2 and to assess how their interactions impact the generation of reactive oxygen species (ROS) and kinetics of ferritin-iron mobilization. Here, voltammetric and amperometric analysis were performed to study the redox behavior of quinones and their interaction with O_2 whereas, spectrophotometric analysis and bio-chemical assays were performed to investigate the in vitro iron release and the impact of in situ-generated ROS. Our result on structure–reactivity of quinone mediators highlight at least three important findings in context of electron mediation capability of the quinones: i.e., electron relay depends on mid-point potential ($E_{1/2}$) value, i.e., quinones with $E_{1/2}$ values lying at a favorable range (not too close and not too far) with respect to NADH exhibited better electron relay, ii. reductive iron release is dictated by molecular structure of relay molecules, i.e., quinones with chelation sites and propensity for H-bonding (favoring semiquinone formation) releases higher amounts of iron, and iii. their relative ability to generate/inhibit ROS viz. superoxide ($O_2^{\cdot-}$) and peroxide (H_2O_2) in situ.

This work signifies the importance of reactivity of quinones toward NADH/O_2 and correlates the contribution of in situ-generated reaction intermediates (SQ) and ROS to the iron-release profiles under both normoxic/hypoxic conditions. Experimental insights of these interactions may strengthen our understanding of the ferritin-iron-release process, in vivo, and their significance in bioenergetics/energy transduction and O_2-based cellular metabolism and toxicity. Further, these insights on quinone-mediated iron mobilization hold promise for addressing iron-overload conditions (chelation therapy) and may offer valuable perspectives on plant/microbial iron acquisition processes to regulate their growth.

Materials and methods

Materials

Quinone derivatives: Benzoquinone (BQ), Hydroquinone (HQ), Napthoquinone (NQ), Menadione (MN), Lawsone (LW), Juglone (JG), Plumbagin (PM), Follin (FL), Anthraquione sulphonic acid (AQS), 3-(N-Morpholino) propane sulfonic acid sodium salt (MOPS-NaCl), Ferrozine (Fz), Nitro blue tetrazolium salt (NBT), Catalase, Horse radish peroxidase (HRP), Bovine superoxide dismutase (SOD), Amplex red were purchased from Sigma Aldrich and β-Nicotinamide adenine dinucleotide disodium salt (NADH) was purchased from SRL. The concentrated stock solutions of all the quinones were prepared in dimethyl sulfoxide (DMSO).

Preparation of recombinant *Mycobacterial* ferritin protein (*Mtb* BfrB)

Overexpression and purification of recombinant *Mycobacterial* ferritin protein (*Mtb* BfrB) was carried out in *Escherichia coli* BL21 (DE3) as per earlier reports [55, 62]. Briefly, *Mtb* BfrB was overexpressed by IPTG induction (0.5 mM) and purified using size exclusion chromatography (Sephacryl S-300). The purity of collected fractions was assessed by SDS-PAGE. After purification, the concentrated *Mtb* BfrB proteins were buffer exchanged with 100 mM MOPS-NaCl buffer (pH 7.0). Native-PAGE was employed to check the cage integrity and the protein concentration was quantified by Bradford assay. The amount of iron present in as-purified *Mtb* BfrB ferritin was estimated (~ 8–10 Fe/cage) by acid cum heat denaturation of the protein cage followed by ferrozine assay [9, 13]. Further, Prussian blue in-gel assay [9] was performed to assess the iron loading ability of the purified ferritin protein.

Preparation of iron loaded *Mtb* BfrB ferritin protein

Mineralized *Mtb* BfrB ferritin protein samples were prepared for iron-release kinetics as previously reported [45]. Iron-loaded ferritin samples (~ 480 Fe/cage), were prepared by adding freshly prepared $FeSO_4$ slution to 2.08 µM of purified *Mtb* BfrB proteins in 100 mM MOPS-NaCl (pH 7.0). The iron-loaded ferritin proteins were incubated for 2 h at 25 °C, followed by 12 h of incubation at 4 °C to ensure complete mineralization. The amount of iron loaded in the mineralized *Mtb* BfrB ferritins was estimated (450 ± 20 Fe/cage) using the ferrozine assay as reported earlier [55].

Mid-point potential of quinone derivatives in neutral aqueous buffer by voltammetry

The efficiency of the quinone derivatives as electron mediators during reductive iron release from *Mtb* BfrB was examined by determining their $E_{1/2}$ values under identical iron-release reaction conditions, using different voltammetric techniques: cyclic voltammetry (CV), square wave voltammetry (SWV), and differential pulse voltammetry (DPV) in neutral aqueous buffer (100 mM MOPS-NaCl; pH 7.0).

Voltammetric analyses of the quinone derivatives (100 µM) were performed using a Versa STAT 4 potentiostat (Princeton Applied Research). The electrochemical setup consists of a three-electrode electrochemical cell: a glassy carbon (working electrode); a Pt wire (counter electrode), and a Ag/AgCl, (reference electrode) [55]. In case of CV, potentials were varied/ramped with a scan rate of 100 mV/s

and the mid-point potential ($E_{1/2}$) values were obtained by averaging both anodic and cathodic peak potential values. In SWV, $E_{1/2}$ values were calculated from the peak positions obtained at the following instrument parameters: pulse height- 25 mV, step height- 0.1 mV, frequency- 100 Hz and scan rate- 10 mV/s. Similarly, in DPV, $E_{1/2}$ values were calculated from the peak positions obtained at the following instrument parameters: pulse height- 25 mV, pulse width- 0.2 s, step height- 10 mV, step width- 2 s and scan rate- 5 mV/s.

Kinetics of NADH oxidation by quinones

Oxidation of NADH by quinone mediators was studied under both aerobic and anaerobic conditions by UV-Visible Spectrophotometry. The kinetics was initiated by mixing NADH with quinone derivatives in 100 mM MOPS-NaCl buffer (pH 7.0). The rate of NADH oxidation ($\Delta A_{340}/\Delta t$) was determined by using initial 2–3 min of data points (linear range) and molar extinction coefficient ($\varepsilon = 6.22\ mM^{-1}\ cm^{-1}$ at $\lambda_{max} = 340$ nm) [55]. The final concentration of NADH and quinone mediators was 160 µM and 100 µM, respectively. For anaerobic experiments all the components, including buffer, were purged with N_2 separately for 1 h prior to the mixing/initiating the kinetics.

Kinetics of dissolved-oxygen consumption

The kinetics of dissolved-O_2 consumption by NADH or NADH/quinone redox couple was investigated for the chosen set of quinone mediators using a Clark electrode (Oxygraph from Hansatech instruments) as reported earlier [13, 21]. In brief, prior to the experiments the current response of the Clark electrode was calibrated with sodium dithionite ($Na_2S_2O_4$) and air-saturated distilled water for 0 and ~250 µM of dissolved O_2, respectively. Dissolved-O_2 consumption was initiated by adding NADH to the buffer solution containing quinones. The kinetics/time courses were recorded in the absence (control reaction: only NADH, 2.5 mM) and presence of quinone mediators (100 µM) in 100 mM MOPS-NaCl buffer (pH 7.0). Similarly, a set of experiments were conducted with pre-incubated samples where, O_2-free solutions of NADH and quinones were incubated for 2 h prior to the kinetics, under similar reaction conditions. The average rates were estimated from the initial linear region (after NADH addition) of the time courses.

Reductive iron-mobilization kinetics

The electron-relay efficiency of quinone mediators and the impact of O_2 were investigated during reductive iron-release process from iron-loaded ferritin proteins by tracking the time-dependent development of charge transfer (MLCT) band at 562 nm, due to formation of Fe^{2+}-ferrozine complex, $[Fe(Fz)_3]^{4-}$ in 100 mM MOPS-NaCl buffer (pH 7.0) at 25 ℃. The concentration and rate of iron release was determined from the absorbance (A_{562}) vs time plot and corresponding molar extinction coefficient at 562 nm ($\varepsilon = 25.4\ mM^{-1}\ cm^{-1}$) [55]. The iron mobilization kinetic experiments were performed under different conditions: i. aerobic, ii. anaerobic, iii. with pre-incubated samples and iv. in presence of ROS scavengers under aerobic conditions. Anaerobic experiments were carried out by purging N_2 gas in each component individually for 1 h prior to their use in iron-release kinetics under anaerobic conditions [55]. In pre-incubated case, O_2 free solutions of NADH and quinones were incubated to obtain reduced form of quinones prior to carrying out reductive iron-release kinetics aerobically. In order to study the effects of $O_2^{\cdot-}$, H_2O_2 and $OH^{\bullet}$, the release of iron from mineralized *Mtb* BfrB ferritins were also carried out under aerobic conditions, separately in the presence/absence of ROS scavengers: 60 U (units) of superoxide dismutase (SOD), 600 U catalase and 500 mM mannitol to the reaction mixture.

The iron-mobilization kinetics was performed by mixing quinone mediators (100 µM), ferrozine (1 mM), to iron-loaded *Mtb* BfrB ferritin (100 µM caged-iron) in aqueous buffer mentioned above. 2.5 mM NADH was finally added to the reaction mixture, to start the reductive iron mobilization.

Quantification of superoxide ($O_2^{\cdot-}$) by NBT assay

In situ-generated superoxide anion ($O_2^{\cdot-}$), during reduction of quinones by NADH was quantified by nitro blue tetrazolium (NBT) assay as per the earlier reports [55]. NBT non-specifically reacts with in situ-generated $O_2^{\cdot-}$ to form a rather stable insoluble reduced product, formazan, which can be solubilized in DMSO and quantified by colorimetry ($\varepsilon = 12.8\ mM^{-1}\ cm^{-1}$ at 530 nm) using a spectrophotometer [55]. Here, formation of formazan was quantified in case of NADH alone (control) or in the presence of quinone analogs in aqueous buffer (100 mM MOPS-NaCl). 2.5 mM NADH was added to a reaction mixture containing 100 µM of quinone mediators and 100 µM of NBT. The insoluble formazan was collected by centrifugation (10,000 rpm, 3 min) of 2 h incubated sample solutions. To specifically estimate the contribution of $O_2^{\cdot-}$ toward NBT reduction, similar experiments were carried out in presence of 60 U of superoxide dismutase (SOD: a superoxide scavenger). The in situ-generated $O_2^{\cdot-}$ was quantified from the difference (in presence and absence of SOD) in the absorbance at 530 nm by eliminating the contribution of NADH alone and NADH/quinone redox couple. Similarly, a set of experiments were conducted with pre-incubated samples and in situ-generated $O_2^{\cdot-}$ was quantified.

Analysis of in situ-generated H_2O_2 by HRP/amplex red assay

H_2O_2 generated in situ by NADH alone (control) or in the presence of quinone analogs in aqueous buffer (100 mM MOPS-NaCl), was analyzed by HRP assay using Amplex Red as a substrate as mentioned in the earlier reports [13, 63]. The oxidized form of amplex red i.e., resorufin ($\varepsilon = 54\ mM^{-1}\ cm^{-1}$ at 571 nm), was recorded by UV-Visible absorption spectrophotometry to quantify the in situ-generated H_2O_2 (resorufin: $H_2O_2 = 1{:}1$) under aerobic conditions. Sample solutions containing amplex red (100 µM), HRP (0.2 µM), and quinone mediator (100 µM) were mixed with NADH (160 µM). Similarly, a set of experiments were conducted with pre-incubated samples and in situ-generated H_2O_2 was quantified.

Results

Voltammetry of quinone mediators in neutral aqueous buffer: mid-point potential values and transient species

The current study uses quinone derivatives as electron mediators to facilitate iron release from *Mtb* ferritin by reductive pathway. During this process, quinones accept 2 e^- from NADH (e^- source) and transfer it to ferritin-iron mineral (e^- sink), either by 1/2 e^- steps. Moreover, the reduced form of these mediators can react with available molecular O_2 in the aqueous buffer. The reaction of these quinone mediators with NADH and ferritin core/O_2 may depend on their mid-point potential ($E_{1/2}$) values. Therefore, different voltammetric techniques were employed here under identical iron-release reaction conditions (100 mM MOPS-NaCl, pH 7.0), to obtain their $E_{1/2}$ values. These values can provide insights on their variable reactivities with NADH and O_2 in generating ROS in situ and may explain their efficiency in reductive iron release from ferritin. Further, cyclic voltammograms (CV) at higher scan rates were recorded to understand the ET mechanism in detail.

The CV of the quinone analogs exhibit well-defined cathodic and anodic peak currents. In neutral aprotic solvent, usually the quinones (Q) undergo two successive, 1 e^- reduction steps generating two separate cathodic and anodic peaks in CV due to the in situ formation and accumulation of semiquinone ($Q^{\cdot -}$) and quinone dianion (Q^{2-}) [64]. In contrast, in aqueous neutral buffer, most quinones undergo rapid $2e^-/2H^+$ redox process (for $Q \Leftrightarrow QH_2$) generating single cathodic and anodic peak (Fig. 2), except for follin (FL) where two anodic peaks were clearly visible at relatively high scan rates (Fig. 2B and Fig. S1). The quinone mediators exhibited variable $E_{1/2}$ values (Fig. 2, Table 1) due to structural differences i.e., substituents attached to the quinone ring (Fig. 1). Moreover, for some quinones $E_{1/2}$ values were found to be different from the reported ones (Table 1). These variations can be attributed to differences in experimental conditions: choice of buffer, pH/techniques employed/type of electrode.

The highest $E_{1/2}$ value ~ 357 ± 30 mV was observed for BQ (i.e., E_{Q/QH_2}), indicating the greater stability of QH_2 due to introduction of aromaticity. The presence of additional benzene ring(s) in naphthoquinone (bicyclic) and anthraquinone sulfonate (tri-cyclic) resulted in lowering of their $E_{1/2}$ value to + 74 mV and − 256 mV, respectively, in comparison to benzoquinone due to extensive resonance. In naphthoquinone derivatives, the position and type of substituents (+I effect of alkyl and −I, +M effect of –OH groups) alter the electron density on the quinone ring to influence their $E_{1/2}$ values. The highest $E_{1/2}$ value in the case of FL can be explained by the presence of two adjacent carbonyl groups (in ortho position with respect to each other) and an electron withdrawing group ($–SO_3^-$). Higher, positive $E_{1/2}$ values for FL, similar to BQ, suggests relatively higher stability of their reduced forms (QH_2) in comparison to oxidized forms (Q) which may influence their electron-relay capability to affect the iron-release process.

The presence of additional electron donating groups ($–CH_3$/–OH) in LW, PM, MN and JG lowers their $E_{1/2}$ value in comparison to the unsubstituted NQ (Table 1). The position of –OH group in JG and LW (appears to be positional isomers) is responsible for the drastic variation in their $E_{1/2}$ values, + 24 and − 136 mV respectively. Moreover, the relative strength of intramolecular hydrogen bonding in β-phenolic quinones (JG) and α-phenolic quinones (LW) might contribute to the differences in their $E_{1/2}$ value and redox behavior (by stabilizing the reduced forms: α-effect). Owing to this stabilization, the $E_{1/2}$ values were shifted toward more positive potentials. The lower $E_{1/2}$ values for PM compared to JG and MN, can be attributed to the presence of an additional electron donating group: $–CH_3$ or –OH. The above results establish that small structural difference among the naphthoquinone derivatives (Fig. 2) leads to large differences in their redox behavior, which may ultimately alter its electron-relay abilities.

Faster NADH oxidation by benzoquinone (BQ) and follin (FL)

The ability of quinones to relay electrons is crucial for ferritin-iron mobilization by the reductive approach and is linked to their reactivity with NADH (e^- source). Therefore, kinetics of NADH oxidation by quinone derivatives was studied by monitoring the change in absorbance at 340 nm (Fig. 3A). A clear difference in absorption profiles

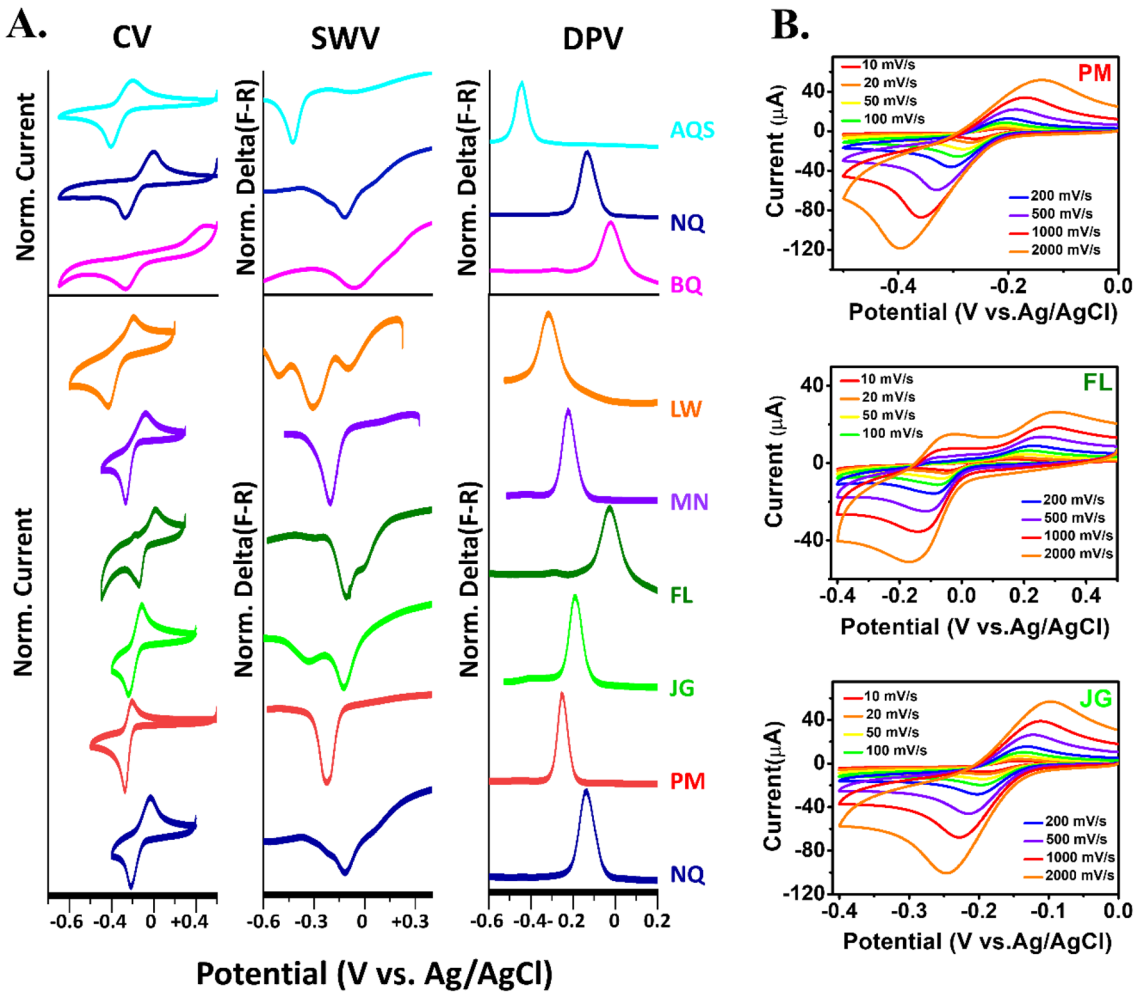

Fig. 2 **A** Voltammetry of quinone derivatives in neutral aqueous buffer. Cyclic voltammetry (CV), square wave voltammetry (SWV) and differential pulse voltammetry (DPV) of quinone mediators (100 μM) in 100 mM MOPS-NaCl buffer (pH 7.0). Signals were normalized for comparison. **B** PM, FL and JG as representative quinones to illustrate the scan rate dependent voltammetry profile

Table 1 Mid-point potential ($E_{1/2}$ for Q/QH_2) of quinone derivatives in 100 mM MOPS-NaCl buffer (pH 7.0)

$E_{1/2}$ (mV vs NHE)						
	Quinones	CV	SWV	DPV	Reported	References
Effect of size	BQ	357 ± 30	247 ± 12	149 ± 37	286	[65]
	NQ	64 ± 16	69 ± 15	52 ± 23	59	[66]
	AQS	− 220 ± 32	− 221 ± 8	− 258 ± 16	− 228	[67]
Effect of substituents	LW	− 136 ± 22	− 162 ± 45	− 169 ± 16	− 87	[68]
	PM	− 32 ± 17	− 21 ± 5	− 34 ± 28	− 77	[69]
	MN	16 ± 23	− 7 ± 11	− 10 ± 46	− 5	[70]
	JG	24 ± 2	38 ± 3	27 ± 2	− 83	[71]
	NQ	64 ± 16	69 ± 15	52 ± 23	59	[66]
	FL	246 ± 26	171 ± 14	180 ± 8	120	[70]

was seen when time-dependent spectra of NADH oxidation were compared under aerobic and anaerobic conditions (Fig. 3A, B). The decrease in 340 nm band was more profound under aerobic conditions with negligible changes in the quinone signature (~410 nm). In spite of faster NADH oxidation, a slow accumulation of reduced form of quinone was seen possibly due to their re-oxidation by O_2. In contrast, under anaerobic condition slow oxidation of

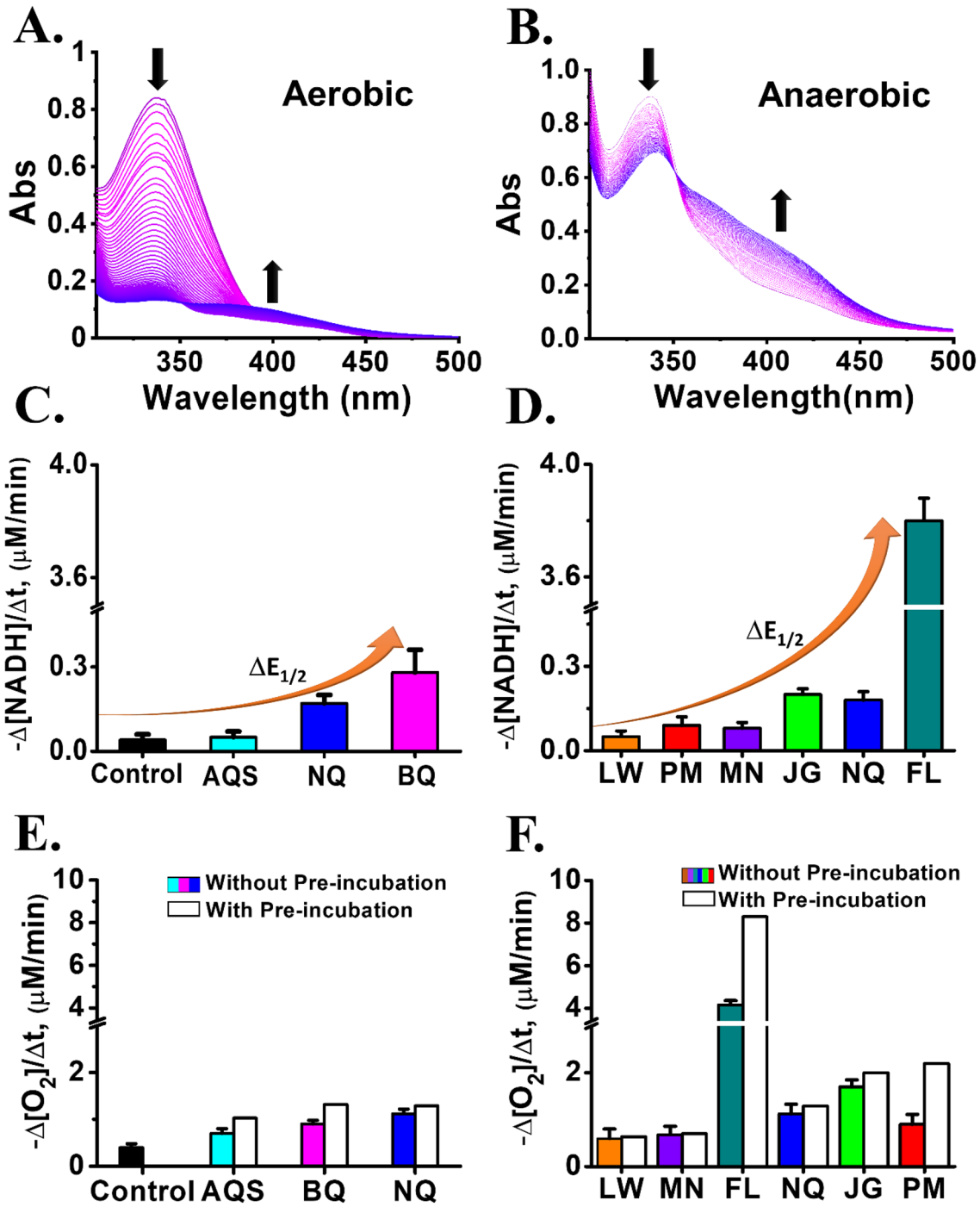

Fig. 3 NADH oxidation and dissolved-O_2 consumption by quinone analogs. Scanning kinetics of NADH oxidation by FL, as a representative quinone derivative, under aerobic (**A**) and anaerobic (**B**) conditions. Control reaction indicates auto-oxidation of NADH in aqueous buffer in the absence of quinone derivatives. (**C**, **D**) Rates of NADH oxidation for different quinones, obtained from the time courses (A_{340nm} vs time. Fig. S4), proportionate to $\Delta E_{1/2}$ values (with respect to NADH). The reaction samples were prepared by mixing of 100 μM of different quinone derivatives with 160 μM of NADH in 100 mM MOPS-NaCl (pH 7.0). (**E**, **F**) are the average rates of dissolved-O_2 consumption by 100 μM of quinones in the presence of 2.5 mM NADH (control reaction: only NADH), determined from the linear region of the time courses after NADH addition (Fig. S5). In pre-incubated case, O_2-free solutions of NADH and quinones were incubated for 2 h prior to carrying out kinetics of dissolved-O_2 consumption. Error bars in (**C-F**) indicate the standard deviation

NADH was observed (Fig. 3B and Fig. S2). Therefore, the relative reactivity of these quinone mediators with NADH and O_2 may influence the reduction/dissolution of iron-mineral core and dictate their overall iron-release process.

Time courses (A_{340nm} vs time) and the respective rates ($-\Delta A_{340}/\Delta t$) indicated that FL oxidized NADH more quickly than any other quinone mediator, possibly due its high $E_{1/2}$ value (Fig. S4 and Fig. 3C, D). The reduced form (two adjacent enol groups, –C–OH) of FL is relatively more stable than its oxidized form (two adjacent electron withdrawing carbonyl groups, –C = O. The mid-point potential difference ($\Delta E_{1/2}$), between NADH and these quinone mediators, increases as we move from AQS to BQ (differential size based arrangement, Fig. 3C) and from LW to FL (differential substituent based arrangement, Fig. 3D). Similarly, an increasing trend is also observed for their NADH oxidation rate (Fig. 3C, D). Thus, we may conclude that most of the quinone mediators in the current study are positioned in the normal region of the Marcus plot, where the rate of ET (NADH oxidation) is directly proportional to its driving force ($\Delta E_{1/2}$).

Naphthoquinone derivatives, follin (FL) and juglone (JG) exhibited faster dissolved-O_2 consumption

Under aerobic conditions, besides the reduction of the ferritin-iron core, there remain additional competitive pathways for the reducing agents/e^- mediators (NADH/quinones) to react with dissolved O_2. Therefore, the relative rates of these competitive pathways dictate the overall iron-release process [45, 55]. Here, we have studied the dissolved-O_2 consumption kinetics by amperometry to investigate the reactivity of the quinones toward O_2, under similar reaction conditions as iron release.

The O_2 concentration in air-saturated aqueous buffer at 25°C and 1 atm is approximately 250 µM [45, 48]. NADH alone (control reaction), consumes less O_2, in comparison to when it is used in combination with quinones (Fig. 3E and Fig. S5). The size of quinones do not play a significant role in the O_2-consumption rate, as BQ and NQ do not exhibit any substantial differences in their kinetic profiles. The relatively higher O_2-consumption rate of BQ and NQ in comparison to AQS may be related to their greater NADH-oxidation rates (Fig. 3E and Fig. S5). Among the NQ derivatives, FL showed faster O_2 consumption, possibly due to similar reasons i.e., higher NADH-oxidation rates (Fig. 3F and Fig. S5). This faster O_2 consumption may affect the iron-release process by lowering the availability of reduced SQ/QH_2 forms of FL. The O_2 consumption rates for all these quinones were found to be higher than their NADH oxidation ability (Fig. S6). This was also reflected in their absorption spectra during NADH oxidation (scanning kinetics) under aerobic conditions; minimal changes were observed for the characteristic quinone bands (Fig. 3A and Fig. S2).

It appears that dissolved-O_2 consumption is influenced by the NADH oxidation ability of quinones. Therefore, to better compare the reactivities of these quinones (in their reduced form) with O_2, N_2-purged solutions of NADH and quinones were pre-incubated for 2 h prior to carrying out kinetics of dissolved-O_2 consumption. All the quinones exhibited enhanced O_2 consumption under pre-incubated cases; with FL showing the highest rate similar to without incubation case (requires half the time to consume all the dissolved O_2) (Fig. 3E, F). A sharp drop in O_2 levels in case of pre-incubated samples indicates the accumulation of reduced forms of quinones in the reaction mixture (Fig. S5C and D).

Impact of size and substituents of quinone based electron mediators on reductive iron mobilization

The kinetics of reductive iron release from mineralized *Mtb* BfrB nanocages was obtained by monitoring the increase in the absorbance at 562 nm due to the formation of $[Fe(Fz)_3]^{4-}$ (Fig. 4A, B). NADH alone i.e., the control reaction without mediator, releases minimal amount of iron, as reported earlier for frog M and other ferritins [55] (Fig. 4A). To facilitate the ET, ferric mineral reduction and iron-mobilization kinetics a set of quinone derivatives has been used as electron mediators, which can participate both as one and two e− donor. Here, the use of quinones in combination with NADH enhanced the iron-release process. To investigate the efficiency of different quinones as electron mediators iron-release kinetics were performed/compared using two sets of quinone which differs in terms of size and substituents.

Impact of size of quinone mediators

Under this category, three quinone mediators: BQ, NQ and AQS were selected based on their differential size to carry out reductive iron mobilization in presence of NADH. Among these, bicyclic NQ released a substantially higher amount of iron from *Mtb* BfrB, as compared to mono-cyclic (BQ) and tri-cyclic (AQS) analogues (Fig. 4C, E). The higher iron release in the case of NQ might be attributed to its efficient e^- mediating ability i.e., possibly it accepts electron from the donor, NADH and readily transfers it to the acceptor, ferritin core. The e^- mediating ability of NQ is reflected in its reduction potential and NADH oxidation kinetics. The $E_{1/2}$ value of NQ (+ 60 mV) is neither very far nor too close to $E_{1/2}$ value of NADH (− 330 mV) and it exhibits NADH oxidation rates intermediate to BQ and AQS. In case of AQS, both the molecular size (steric hindrance in entering the ferritin cavity) and slower NADH oxidation due to low $E_{1/2}$ values (− 220 mV) may contribute

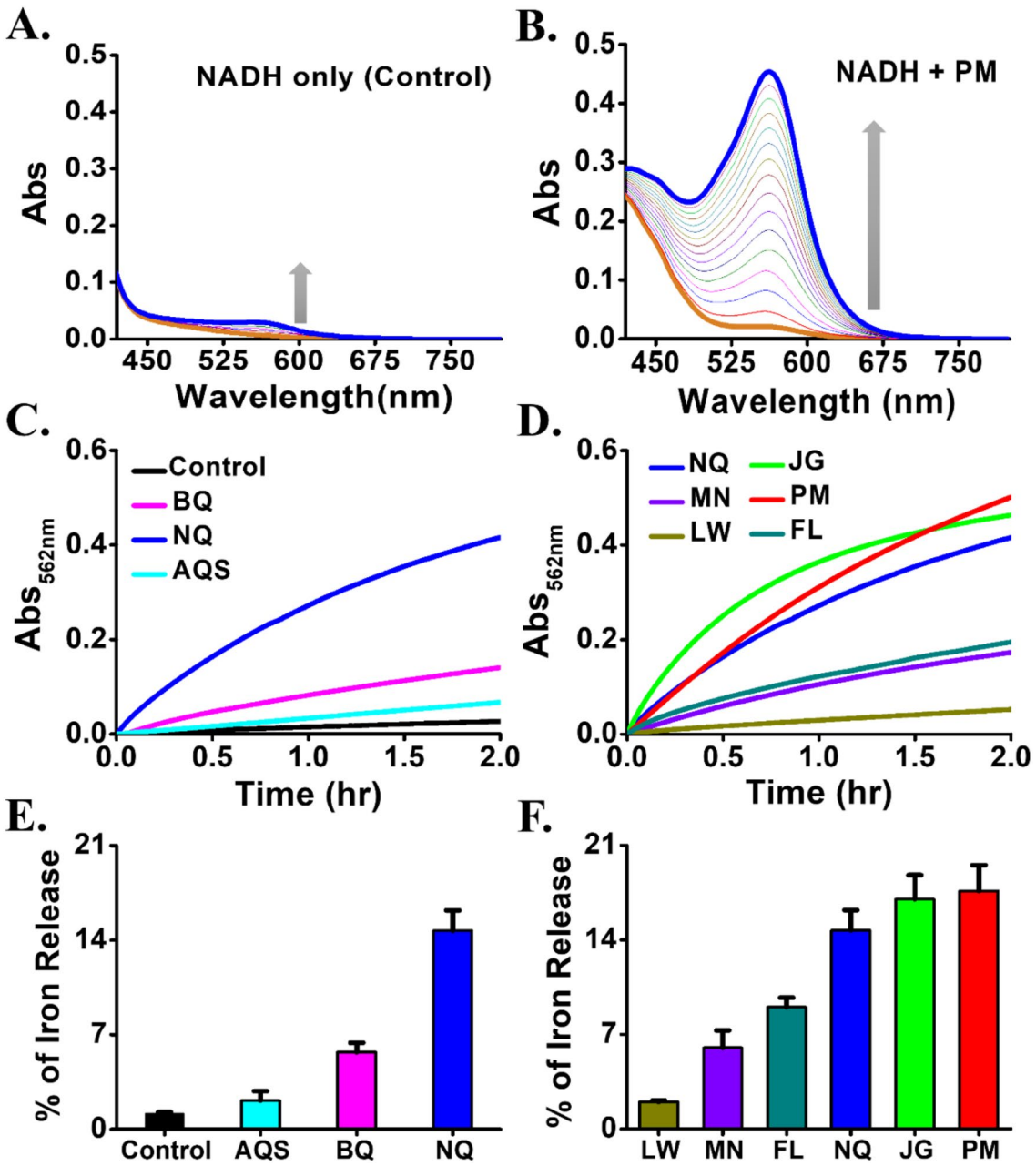

Fig. 4 Impact of size and substituents of quinone derivatives on reductive iron mobilization from *Mycobacterial* ferritin nanocage. Iron mobilization from *Mtb* BfrB indicated by appearance of a 562 nm MLCT-band in UV–Visible absorption spectra due to the formation of $[Fe(Fz)_3]^{4-}$ complex, in the presence of physiologic reducing agent, NADH (**A**) and in combination with a representative electron mediator, PM (**B**). Comparison of kinetic traces of iron mobilization by a set of quinone derivatives based on (**C**) size and (**D**) substituents. Control reaction indicates iron release from ferritin nanocages in the absence of any quinone mediator (only by NADH). (**E–F**) Percentage of iron release after 2 h of reaction. The reaction samples were prepared by mixing of 0.2 µM mineralized ferritin cage (containing 100 µM caged iron, 500 Fe/cage) with 1 mM ferrozine and 100 µM of quinones mediators in 100 mM MOPS-NaCl (pH 7.0) followed by the addition of 2.5 mM NADH

to less iron release. However, for BQ the stability of reduced form i.e., hydroquinone QH_2, which is reflected in its high $E_{1/2}$ value (+357 mV) (Table 1), possibly explains its slower iron-release pattern as compared to NQ, despite having a smaller size.

Impact of substituents in naphthoquinone derivatives

Among the naphthoquinone derivatives, JG and PM releases maximum amount of iron, despite exhibiting slow NADH

oxidation (Fig. 4D, F). This indicates their better electron-relay efficiency and the possibility of involvement of other factors toward higher iron release. The extent of iron release can be correlated based on the nature of the functional group attached to NQ. The two NQ derivatives: JG and PM are structurally exceptional due to the presence of a hydroxyl (–OH) group at the non-quinone aromatic ring (Fig. 1), which introduces an iron chelating/coordinating site (Fig. S13). These two NQ derivatives are structurally similar, except for the fact that PM has an additional methyl ($–CH_3$) group attached at the C-2 position. Due to this structural difference, both JG and PM showed different $E_{1/2}$ values, which may have influenced their e^- mediating abilities to a certain extent, which is clearly reflected in their differential initial rates (Fig. S7, Table S1).

FL, MN and LW exhibited a slower rate of iron release compared to NQ, which may reflect their inefficiency in electron relay (either slow-NADH oxidation or slow mineral reduction) and can be correlated with their $E_{1/2}$ values. As compared to NQ, FL has a higher positive reduction potential ($E_{1/2}$ ~ 246 mV) whereas LW has a higher negative reduction potential ($E_{1/2}$ ~ − 136 mV). The high and low $E_{1/2}$ value may affect the electron-relay ability (accepting/donating) of these NQ derivatives (FL and LW) to influence iron-release kinetics.

Moreover, the drastic difference in the iron-release efficiency between LW and JG (positional isomers) further emphasizes the impact of –OH group at C-5 position. The presence of $–CH_3$ group in MN at C-2 position or the lack of –OH group at C-5 position (unlike JG and PM), possibly makes MN an inefficient electron mediator for reductive iron mobilization, despite its favorable $E_{1/2}$ values. Further, when menadione sodium bisulfite (MNS) was compared with MN, iron release was found to be similar (Fig. S8).

Further, slower iron release by FL maybe due to its faster O_2 consumption (Fig. 3F), which can lower the availability of its reduced SQ/QH_2 forms or its poor ET ability to the ferritin mineral core. In contrast, JG shows both faster O_2 consumption and iron release, reflecting its better ET/mediating efficiency. This further supports that JG and PM are better electron-relay molecules for reduction of ferritin mineral core despite exhibiting high rates of dissolved-O_2 consumption.

Impact of dissolved O_2 on the reductive iron mobilization

The iron-mobilization experiments conducted under anaerobic conditions, exhibited an enhanced amount of iron release in comparison to aerobic conditions (Fig. S9). Anaerobic experiments were carried out by purging N_2 gas in each component of all the samples individually for 1 h prior to monitoring iron-release kinetics under anaerobic conditions. PM, JG and NQ showed higher amounts of iron mobilization from ferritin core both in aerobic and anaerobic condition (Fig. S9) and similar trends were also observed for other quinones. Under anaerobic conditions, the 2 e^- transfer from NADH to quinone (Q) leads to quinol (QH_2), which may undergo comproportionation reaction with Q to form SQ. Both these 1/2 e^- reduced form of quinone derivatives (QH_2/SQ) can participate in reduction/dissolution of iron-mineral core to facilitate iron mobilization. However, under aerobic condition, O_2 can compete with ferritin-iron mineral to oxidize the QH_2/SQ and thus can minimize the iron mobilization process. Further, this O_2 may initiate the re-oxidation of the Fe^{2+} (formed by the reduction of Fe^{3+} mineral). Moreover, the reduction of dissolved O_2 in aerobic conditions may lead to the formation of ROS species ($O_2^{\cdot-}$/H_2O_2/$OH^{\bullet}$) which can further play a role in affecting the iron-mobilization kinetics.

Impact of in situ-generated ROS species ($O_2^{\cdot-}$/H_2O_2/$OH^{\bullet}$) on the reductive iron mobilization

Reductive iron release from ferritin nanocages can be influenced by in situ-generated reactive oxygen species (ROS) such as $O_2^{\cdot-}$, H_2O_2 and $OH^{\bullet}$. To study their impact, iron-release experiments were carried out in presence and absence of ROS scavengers viz. SOD, catalase and mannitol.

SOD is one of the fastest anti-oxidative enzyme, well-known to catalyze the dismutation reaction of $O_2^{\cdot-}$ to H_2O_2 and O_2. In presence of SOD the iron release by most of the quinone mediators (except FL) was seen to be retarded (Fig. 5A, B). This observed inhibition of iron release can be possibly explained by: i. decrease in the amount of $O_2^{\cdot-}$, which otherwise acts as a reducing agent to facilitate iron reduction/mobilization, or ii. production of H_2O_2, a relatively strong oxidant than O_2, or iii. a combined impact of $O_2^{\cdot-}$ consumption and H_2O_2 generation. As, $O_2^{\cdot-}$ mediated iron release is reported to be relatively less efficient, inhibitory effect of H_2O_2 may be the predominant factor in dictating the rates of iron release. FL exhibited similar iron-release profiles both in presence and absence of SOD, possibly due to two opposing effects: (1) inhibitory effect of H_2O_2 and (2) enhancing effect of $FL_{SQ.}$ Appearance of two anodic peaks at high scan rates, (CV data, Fig. 2B) possibly supports the formation/accumulation of semiquinone species in FL.

In contrary to SOD, presence of catalase promotes iron release, by lowering the H_2O_2 amount in the reaction medium (Fig. 5C, D). However, FL showed a minimal increase and a clear anomaly was observed in case of BQ, which significantly inhibited the iron release. Hydroquinone, the reduced form of BQ, can inhibit the catalase activity (prevents H_2O_2 detoxification) [72] and inhibit iron release. Further, iron-release experiments were carried out with

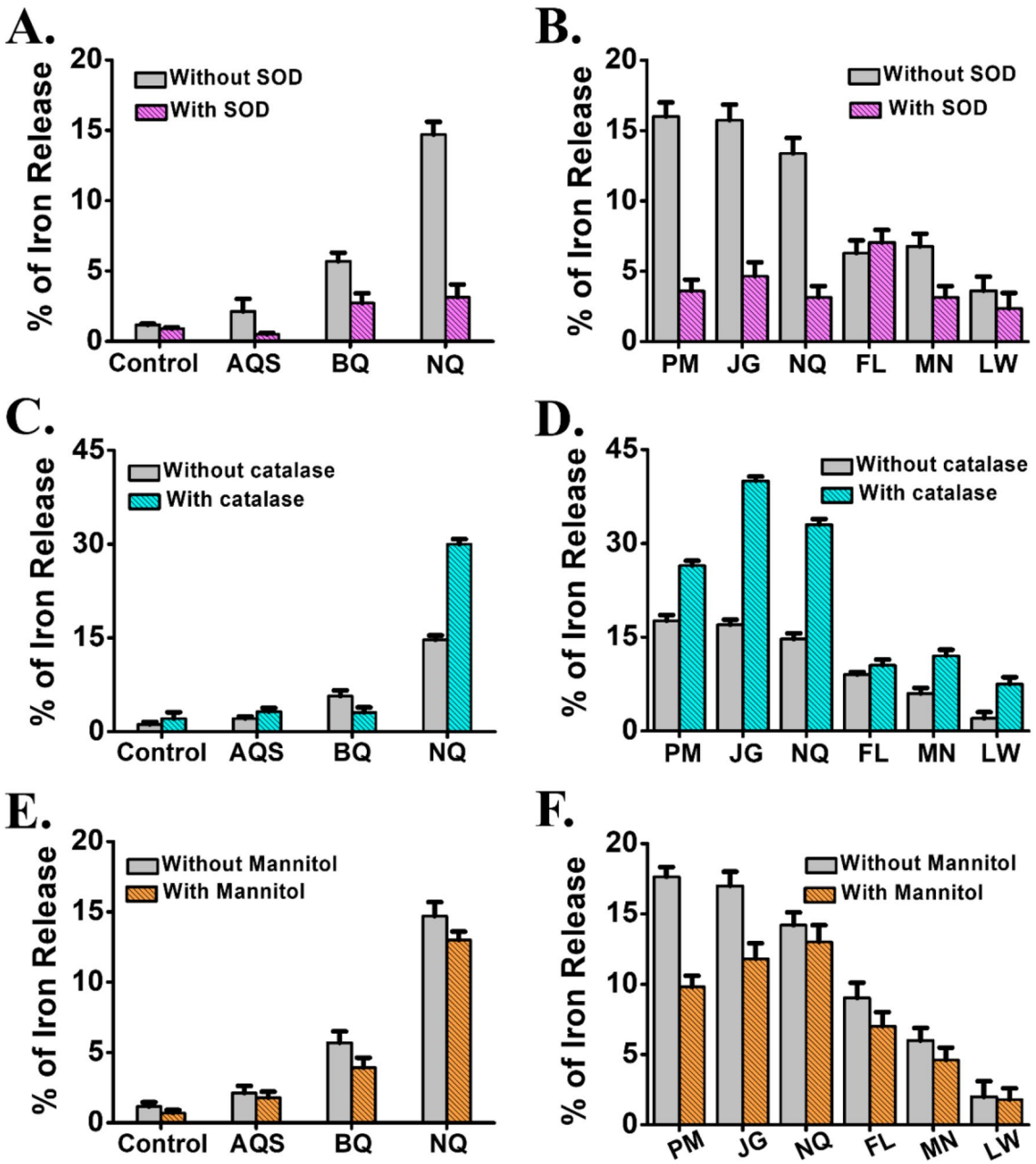

Fig. 5 Effect of SOD, Catalase and Mannitol on quinone mediated reductive iron release from *Mtb* BfrB. Percentage of iron release after 2 h, were computed from the absorbance vs time plot at 562 nm (Fig S10) and compared in the presence and the absence of ROS scavengers. Iron release from *Mtb* BfrB was initiated by adding 2.5 mM NADH to the reaction mixture containing 100 µM caged iron, 100 µM quinone and 1 mM ferrozine in 100 mM MOPS-NaCl buffer (pH 7.0)

external addition of H_2O_2 where it inhibits the iron-release kinetics. Addition of catalase was seen to minimize the H_2O_2 effect which supports our observation (Fig S11).

Interestingly, in the presence of mannitol (free radical scavenger), the iron-release was found to be slightly lower (Fig. 5E, F). This observation maybe possibly linked to the following factors: i. $OH^{\bullet}$ may trigger alterations in the ferritin structure or promote the generation of quinone from tyrosine resulting in a higher iron-mobilization, and ii. the hydroxyl groups in mannitol may compete with ferrozine for Fe^{2+}.

Detection/quantification of in situ-generated H_2O_2 and $O_2^{\cdot-}$ during the reduction of quinones by NADH under aerobic conditions

The reaction between NADH and quinones consume significant amounts of dissolved O_2, which leads to the generation of ROS species in the reaction medium. 1/2 e^- reduction of O_2 by partially/completely reduced quinone species (SQ/QH_2) can form $O_2^{\cdot-}$/H_2O_2 species. Moreover, both catalytic and non-catalytic disproportionation of in situ-generated $O_2^{\cdot-}$ can produce H_2O_2. Presence of H_2O_2 and $O_2^{\cdot-}$ are known to alter the iron-release kinetics. Therefore, horse radish peroxidase (HRP) and nitro blue tetrazolium (NBT) assays were performed to quantify the H_2O_2 and $O_2^{\cdot-}$ species generated during NADH/quinone reaction under aerobic conditions to explain the efficiency/mechanism of these mediators (Fig. 6).

Specific quinones (BQ, NQ, JG and FL) inhibit in situ *generation of H_2O_2 by NADH*

The fate of dissolved O_2 consumed during the reduction of quinones by NADH under aerobic conditions was investigated by analyzing the in situ generation of H_2O_2, using HRP assay. Figure 6A–C shows a gradual increase in absorbance at 571 nm due to formation of resorufin with time (development of pink color upon oxidation of amplex red) in samples containing HRP, NADH (160 µM) and quinones (100 µM). Interestingly, the control reaction (only NADH), generated a significant amount of H_2O_2 (~ 24 µM), which might a possible reason for lower iron release in the absence of quinone mediators. Similar amount of H_2O_2 was detected when MN, LW and AQS were added to NADH, indicating their minimal impact on H_2O_2 generation and can be correlated to their lower iron-release abilities. Although, similar amount of H_2O_2 was detected when PM was added to NADH, its higher iron-release abilities can be related to other factors such as favorable $E_{1/2}$ values and structural factors. However, BQ, NQ, JG and FL inhibit the generation/accumulation H_2O_2 in the solution mixture, which ultimately contribute to the enhanced the iron release.

JG and FL generate more amount of $O_2^{\cdot-}$ during reaction with NADH

NBT assay quantifies the concentration of formazan (λ_{max} ~ 530 nm in DMSO), an insoluble two electron reduced species formed by the reduction of NBT in the reaction mixture. However, the reduction of NBT can be achieved by NADH and in situ-generated SQ/QH_2 and $O_2^{\cdot-}$. As, NBT reduction is not exclusive to $O_2^{\cdot-}$, quantification of $O_2^{\cdot-}$ is performed both in the presence and absence of superoxide dismutase (SOD) (Fig. 6D). Maximum amount of $O_2^{\cdot-}$ formation was observed in FL and JG (Fig. 6E). The in situ-generated $O_2^{\cdot-}$ amount can be correlated to their higher dissolved-O_2 consumption ability (Fig. 3F). In contrast to H_2O_2 generation, in the control reaction, NADH alone generated insignificant amount of $O_2^{\cdot-}$ due to its 2 e^- donating capability. This demonstrates the role of quinones on in situ $O_2^{\cdot-}$ formation.

Impact of quinone, quinol and pre-incubated quinones (with NADH) on iron mobilization

The reductive iron-release kinetics by addition of oxidized form of quinone to reaction solutions containing NADH indicated their electron mediating ability (electron accepting from NADH and transferring to ferritin-iron mineral). The iron mineral reduction (ET) efficiency of these quinone derivatives was further compared by using the reduced form of these quinones (QH_2: quinol). Therefore, hydroquinone (HQ, commercially purchased), the reduced form of BQ was used directly, as electron source cum mediator for the iron-release process. Similarly, the reduced form of all the quinones was prepared by incubating with NADH prior to the kinetic experiments (see methods section).

When hydroquinone (HQ) was used (with/without NADH), nearly threefold decrease in iron release was observed as compared to BQ mediated reductive pathway (Fig. 7A). Differences in iron mobilization by HQ and BQ possibly indicate the differential involvement/generation of ROS/semiquinone (SQ) in situ. In the control and pre-incubated sample, more amounts of H_2O_2 was detected, possibly because of 2 e^- transfer from NADH/QH_2 to O_2, which is shown to inhibit iron release (Fig. 7D, F). Whereas in samples without pre-incubation more amount of $O_2^{\cdot-}$ was generated, indicating the possible involvement of SQ. Both SQ and $O_2^{\cdot-}$ are better reductants than QH_2, which supposedly enhances iron release by 1 e^- reduction of the iron-mineral core. Similar to HQ, when other quinones were pre-incubated with NADH and used for iron-release kinetics, lower iron release was observed compared to cases without pre-incubation (Fig. 7B–D and Fig. S12). The amount of $O_2^{\cdot-}$ and H_2O_2 detected in this experiment not only relates to the iron-release profiles of the quinones (Fig. 7) but may also imply the generation of transient SQ species.

Discussion

Controlled iron release from intact ferritin is crucial for providing steady supply of iron for essential physiologic processes while dodging the negative effects of excess free iron[73, 74]. The reductive pathway is recognized as a

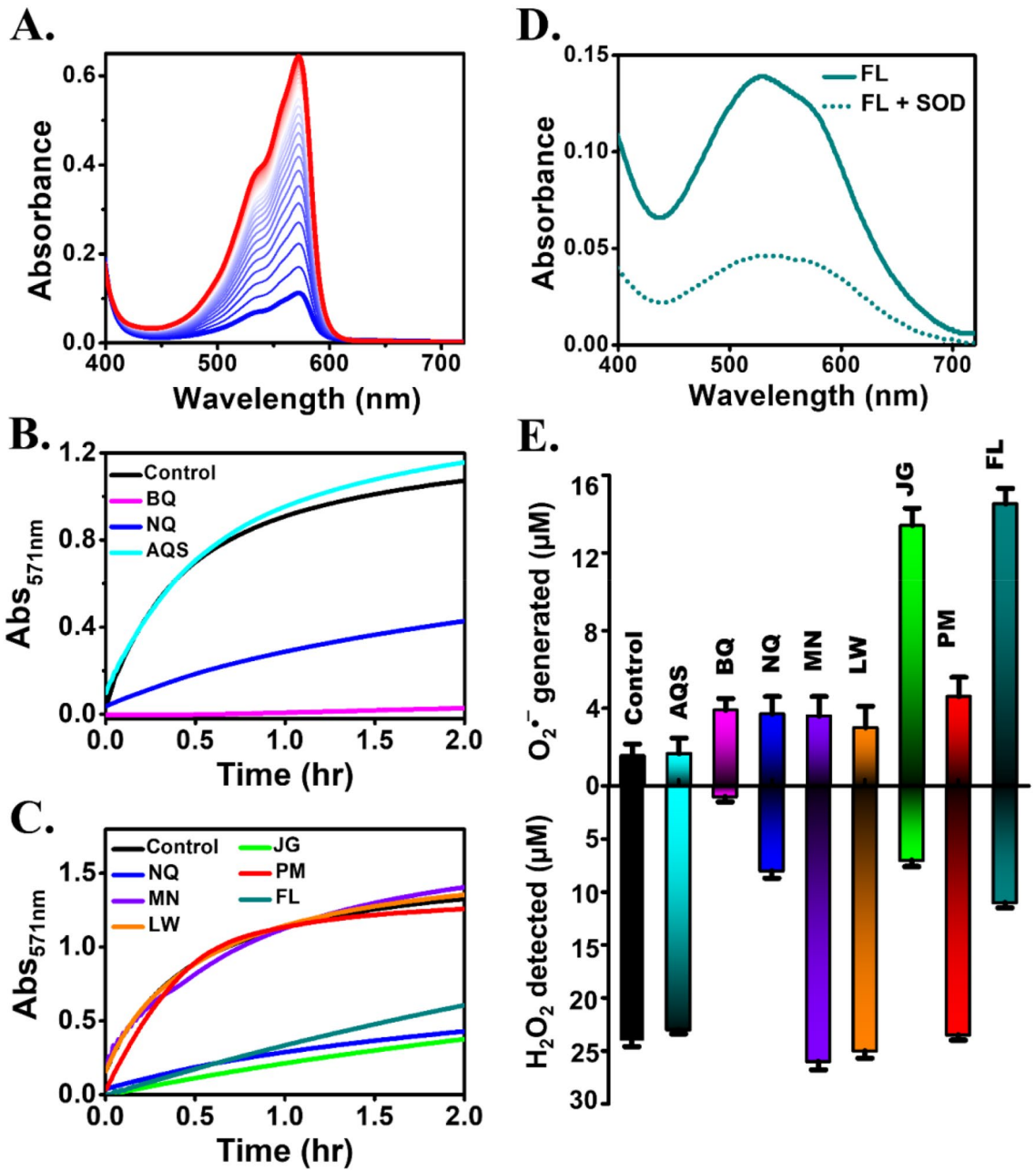

Fig. 6 Detection/quantification of in situ-generated H_2O_2 and $O_2^{\bullet-}$ during reduction of quinones by NADH. **A** Representative of H_2O_2 detection by HRP assay. **B** and **C** Time courses of formation of resorufin by NADH alone (control) and in combination with quinone analogs. **D** NBT assay for quantification of $O_2^{\bullet-}$ generated by FL (a representative of electron-relay molecule) in presence of NADH (electron donor). To quantify $O_2^{\bullet-}$ generated in situ the NBT assay was performed both in presence and absence of SOD (60 U). **E** In situ-generated H_2O_2 (resorufin: $H_2O_2 = 1:1$) and $O_2^{\bullet-}$ (formazan: $O_2^{\bullet-} = 1:2$) detected during reduction of quinones by NADH

possible viable mechanism for releasing iron from these cellular storehouses in vivo [34, 75, 76]. This pathway requires the participation of reducing agents which donate electrons either through indirect long-range ET via the protein cage by interacting with the external surface of ferritin or may directly reduce the mineral core after entering into the nanocavity [55, 77–79]. Mineral core reduction is possibly the rate limiting step; factors which enhance this step can facilitate the iron-release process.

In corroboration with previous reports on frog M and other ferritins [45, 55] reductive mobilization of ferritin iron from *Mtb* BfrB demonstrate that despite having a large negative reduction potential, physiologic reducing agent NADH could only release a minimal amount of iron in a slow

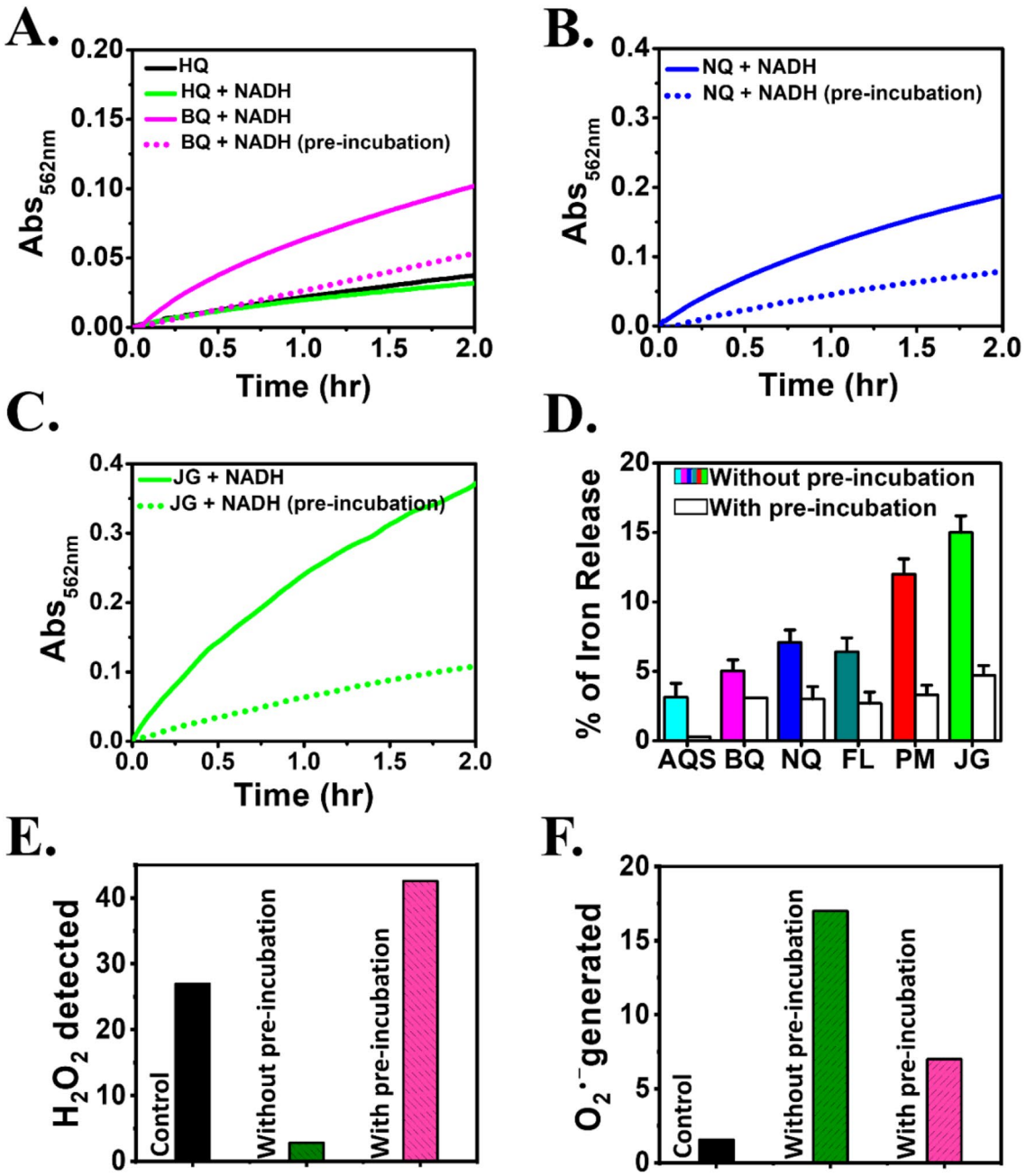

Fig. 7 Reductive iron release with and without pre-incubated quinones. **A** Comparison of reductive iron release mediated by quinone (BQ), quinol (hydroquinone: HQ) and pre-incubated BQ (incubated with NADH under anaerobic conditions). Kinetic traces of iron mobilization by representative quinone derivatives with and without pre-incubation: (**B**) NQ and (**C**) JG. Percentage of iron release after 2 h of reaction (**D**). Error bars in (**D**) indicates the standard deviation. Detection/quantification of: (**E**) $O_2^{\cdot-}$ and (**F**) H_2O_2, generated in situ during reduction of JG by NADH in respective samples

pace. This observation is possibly due to various reasons: i. NADH participates in ET as a two e^- donor, ii. Columbic repulsions between negatively charged NADH and *Mtb* BfrB (theoretical pI ~ 4.83), iii. the relatively larger size of NADH as compared to the narrow BfrB pores [55] Hence, an indirect pathway of ET is presumed in the case of NADH, via the redox active amino acid residues (electron-relay stations) located in the ferritin protein shell. Moreover, in this work, a significant in situ generation of H_2O_2 by NADH (in control reaction) was observed in aqueous buffer, which consequently inhibited the reductive iron dissolution/mobilization (Fig. 8A. Pathway 2). Therefore, quinones were employed as electron mediators in conjugation with NADH to enhance the mineral core reduction by facilitating both 1/2 e^- transfer

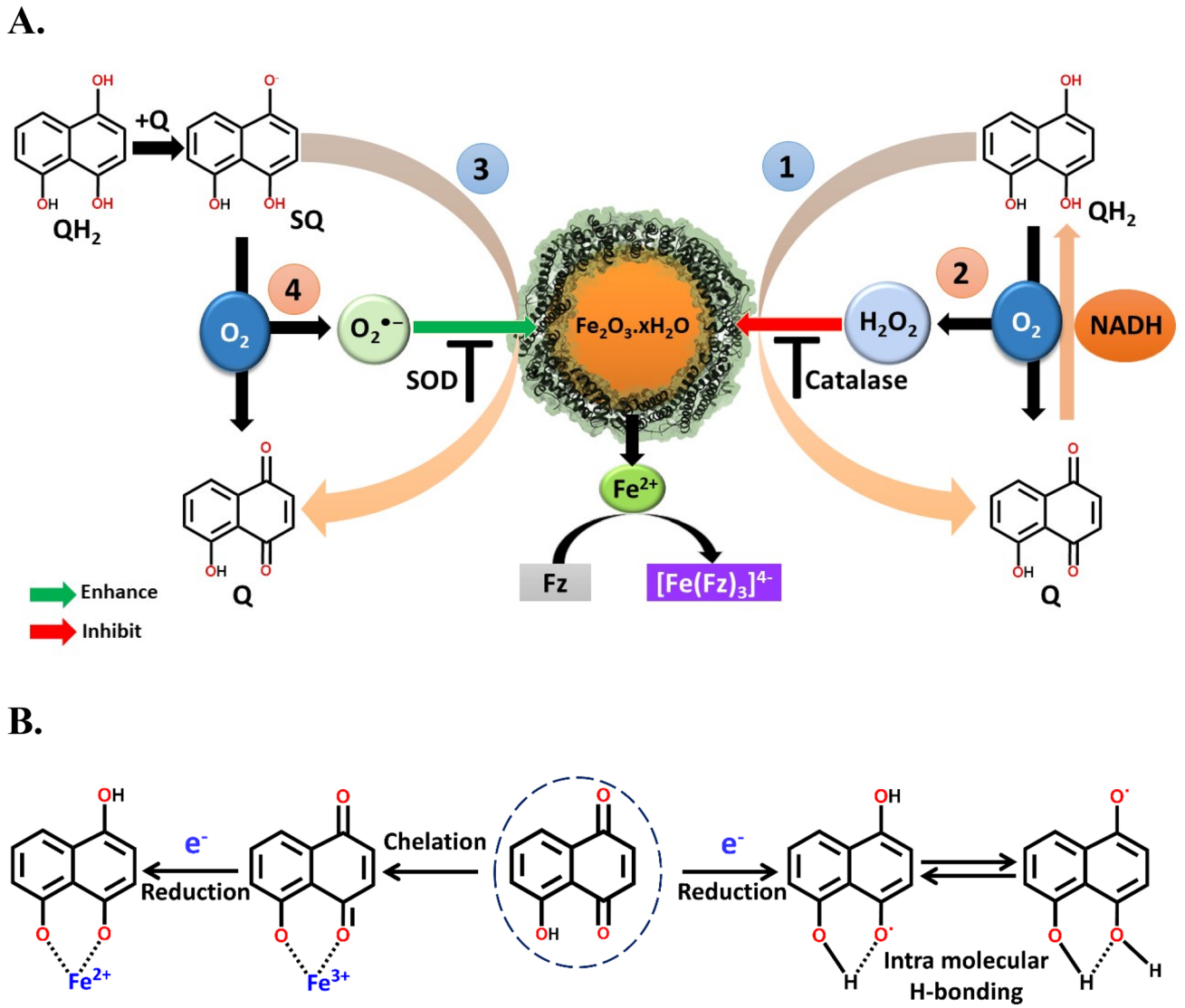

Fig. 8 **A**. Competitive mechanisms of quinone-based reductive iron mobilization from ferritin: Impact of quionol (QH_2), semiquinone (SQ), peroxide (H_2O_2), and superoxide radical anion ($O_2^{\bullet-}$). The two electron source NADH and quinol participate in iron-mineral core reduction (**1**) as well as react with O_2 in situ to generate H_2O_2, that potentially inhibits iron release; catalase facilitates iron release by disproportionation of H_2O_2 (**2**). Quinol and quinone undergoes a comproportionation reaction to give semiquinone (SQ), which may participate in long range ET (**3**) or generate $O_2^{\bullet-}$ intermediate in situ (**4**) to reduce the ferritin mineral core, both via 1 e^- transfer mechanisms. SOD inhibits iron release either by scavenging $O_2^{\bullet-}$ or generating H_2O_2 by disproportionation. **B**. Coordination/reduction of iron and intramolecular H-bonding by quinones. Left: Quinones (JG and PM) with iron coordinating sites promote Fe^{3+} reduction. Right: H-bonding may favor the generation of semiquinone species to influence the reductive iron release

processes (Fig. 8A. Pathway 1 and 3). Here, the differential reactivity of quinone derivatives with NADH and O_2/ferritin and their ability to generate/inhibit ROS/semiquinone intermediate was investigated in detail to explain their iron-release efficiency.

Despite oxidizing NADH faster, BQ and FL show a moderate/intermediate iron-release profile due to the following reasons: i. high $E_{1/2}$ values, lying very far from NADH, favoring their reduced forms (QH_2) in comparison to oxidized forms (Q), and ii. faster O_2 consumption which results lower availability of reduced forms to participate in mineral core reduction. Similarly, AQS and LW with $E_{1/2}$ values close to NADH, shows less/slow NADH oxidation (less reduced species), and ultimately less iron release. However, PM, JG with $E_{1/2}$ values lying at an intermediate range with respect to NADH, are found to display better electron shuttling ability as reflected in their iron-release profiles. Therefore, $E_{1/2}$ values of these mediators are one of the key factors in determining the reductive iron mobilization.

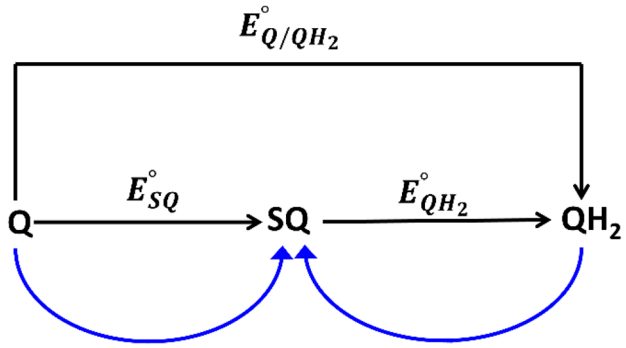

Scheme 1 Comproportionation of quinone (Q) and quinol (QH_2) to generate semiquinone (SQ). E° values indicate the respective standard reduction potentials

PM and JG released maximum amount of iron from *Mtb* BfrB, despite exhibiting slow NADH oxidation and can also be linked to the presence of an iron chelating/coordinating site ('OH' group in C-5 position) (Fig. 8B, left). Naturally, bacteria secrete siderophores as specialized molecules to chelate and acquire iron from their surroundings. Siderophores possess distinct iron-binding sites, such as catecholate and hydroxamate-based moieties, exhibiting a remarkably high and specific affinity for Fe^{3+} chelation (K_{eq} as high as 10^{50}) [39, 80, 81]. Similar to siderophores, PM and JG, also demonstrate iron-chelating properties, owing to their favorable structural features (oxidized: C–OH, C=O and reduced: C–OH, C–OH), which may facilitate the chelation and mineral core reduction to enhance ferritin-iron release (Fig. 8B, left). Some of these quinone molecules are synthesized by plants to acquire iron and other nutrients [58, 82].

Iron release was higher for all quinones under anaerobic conditions in comparison to aerobic conditions (samples without pre-incubation conditions > pre-incubated samples). Presence of dissolved O_2 delays the reductive iron-release process by re-oxidizing the reduced Fe^{2+}/quinones (QH_2/SQ) and promoting H_2O_2 formation. In pre-incubated sample, nearly threefold decrease in iron release was observed as compared to samples without pre-incubation and can be possibly linked to generation/detection of higher amount of H_2O_2 (strong oxidant) in pre-incubated sample (Fig. 7).

The 2 e^- transfer from NADH to quinone (Q) leads to hydroquinone (QH_2), which may undergo comproportionation reaction with Q to form semiquinone (SQ) (Scheme 1). SQ radicals can participate in 1 e^- transfer reactions to facilitate reduction of the ferritin mineral core. Further, this species can be scavenged by molecular O_2 to produce $O_2^{\cdot-}$, which can also reduce the mineral core but possibly at a slower rate [55, 83].

The extent of semiquinone formation can be better understood by using the Nernst equation (at equilibrium), which states that for comproportionation reaction the equilibrium/stability constant is directly proportional to the concentration of semiquinone species (i.e., $K_{eq} \propto$ [semiquinone]). K_{eq} values obtained from the Nernst equation for JG (~ $10^{-4.02}$) and PM (~ $10^{-3.90}$) (Table 2) were higher as compared to other quinones (except FL, ~ $10^{-2.91}$), which possibly reflects a relatively higher formation of SQ.

$$\text{Nernst Equation: } E^{\circ}_{\text{cell}} = E^{\circ}_{\text{SQ}} - E^{\circ}_{\text{QH}_2} = \frac{RT}{nF} ln K_{\text{eq}} = \frac{RT}{nF} ln \frac{[SQ]^2}{[Q].[QH_2]}$$

The –OH group at C-5 position (in PM and JG) may drive the formation of SQ/QH_2 by intramolecular hydrogen bonding resulting in a six-membered ring structure (Fig. 8B, right). In contrast, for LW having C-2 OH group, a relatively weaker five-membered ring structure can be expected. JG and LW despite being positional isomers show different reactivity toward NADH/O_2 and ferritin mineral reduction. Our analysis supports the earlier reports that JG can produce more amount of SQ than LW [85] which ultimately influence

Table 2 Reduction potentials (Q/SQ; SQ/QH_2) for quinone derivatives (mV vs NHE) and their respective K_{eq} for comproportionation reaction at pH 7.0

Quinones			Comproportionation	
	E°_{SQ}	$E^{\circ}_{QH_2}$	$E^{\circ}_{cell} = E^{\circ}_{SQ} - E^{\circ}_{QH_2}$	$K_{eq} = \frac{[SQ]^2}{[Q][QH_2]}$
Benzoquinone (BQ)	99	473	− 374	$10^{-6.32}$
Naphthoquinone(NQ)	− 140	280	− 420	$10^{-7.10}$
Juglone(JG)	− 95	143	− 238	$10^{-4.02}$
Plumbagin(PM)	− 156	76	− 238	$10^{-3.92}$
Follin(FL)	68	240	− 172	$10^{-2.91}$
Menadione(MN)	− 203	193	− 396	$10^{-6.70}$
Lawsone (LW)	− 415	143	− 136	$10^{-9.44}$
Anthraquinone sulphonate (AQS)	− 390	− 76	− 314	$10^{-5.31}$

E°_{SQ} is the mid-point potential for Q/SQ, obtained from [84]

$E^{\circ}_{QH_2}$ is the mid-point potential for SQ/QH_2, calculated from E°_{SQ} and E°_{Q/QH_2} (from Table 1) using the Latimer diagram $E^{\circ}_{(QH_2)} = 2E^{\circ}_{(Q/QH_2)} - E^{\circ}_{SQ}$

K_{eq} values were obtained from the Nernst equation

the iron-release kinetics. PM also exhibits H-bonding via its –OH group at C-5 position but its reactivity toward NADH, O_2, and ferritin mineral lies intermediate to that of JG and MN, due to the presence of an additional $–CH_3$ group at C-2 position.

ROS such as hydrogen peroxide (H_2O_2) and subsequent hydroxyl radicals ($OH^{\bullet}$) can be generated via multiple pathways, during quinone-NADH interaction to influence reductive iron release. The inhibitory effect of H_2O_2 towards reductive iron mobilization was exhibited in control reaction, pre-incubated samples and quinones such as AQS, MN and LW, where higher amounts of H_2O_2 was detected. Less amounts of H_2O_2 were detected in JG and NQ as compared to the control, which correlates well with their iron-release profiles. Upon addition of catalase, the iron release was enhanced/rescued, which further supports the inhibitory effect of H_2O_2.

In the presence of SOD, all the quinones show lesser iron release (except FL) possibly by scavenging the 1 e^- donor $O_2^{\bullet-}$ or generating the 2 e^- oxidant H_2O_2, by its catalytic disproportionation reaction. FL exhibited similar iron-release profiles both in presence and absence of SOD, possibly due to two opposing effects: (1) inhibitory effect of H_2O_2 and (2) enhancing effect of FL_{SQ}. FL in aqueous buffer exhibited two anodic peaks, similar to non-aqueous/aprotic solvents, under high scan rates (Fig. 2B), possibly indicating the accumulation of FL_{SQ} species. FL_{SQ} can be generated by comproportionation reaction between FL_{Red} and FL_{Ox}, possibly facilitated either by in situ-generated H_2O_2 or structural stabilization of FL_{SQ} by two adjacent C = O groups (1,2 naphthoquinone) in aqueous buffer. Interestingly, FL also exhibited similar iron-release profiles both in presence and absence of catalase, possibly due to two counter effects: (1) detoxification of H_2O_2 and (2) lower accumulation of FL_{SQ}.

In case of BQ, its reduced form can inhibit the catalase activity (possibly by reducing the Compound I) and minimize H_2O_2 detoxification [72].Moreover, interactions between SQ/QH_2 and catalase might lower the effective concentration of reduced BQ species to inhibit in the iron-release kinetics. This anomalous behavior of BQ and FL toward ferritin-iron release can be a future prospective of this work.

In nature, plants/microbes synthesize variety of quinones that help to facilitate iron/nutrient acquisition and are critical components of the respiratory chain both in aerobic and anaerobic systems. As quinones are active components of natural ET networks, this study may be helpful in finding the ET pathways followed in vivo. Enhanced iron release under anoxic conditions can be linked to bacteria adapting to the low-oxygen conditions that can utilize Fe^{3+}-compounds as terminal electron acceptors, similar to how oxygen is used in aerobic respiration, a phenomenon known as "iron respiration" [41, 42]. For intracellular pathogens like *Mtb,* quinones or similar electron mediators can play a critical role in mobilizing iron from *Mtb* ferritins or acquiring iron from host under iron scarcity. Further, our findings would be helpful to choose the appropriate quinones with minimal ROS generation tendency while being efficient in iron mobilization for applications toward removal of excess iron under iron-overload conditions. Insights on the reactivity of quinones with $NADH/O_2$ and their electron-relay efficiency can be exploited toward energy transduction, design of microbial fuel cells and catalytic applications [60].

Conclusion

In the current report, the differential redox activity of quinone derivatives, their reactivity with $NADH/O_2$ and their ability to generate/inhibit ROS/semiquinone intermediate was investigated. Further, their tuneable electron-relay ability was exploited in mobilizing iron from *Mycobacterial* ferritins by NADH. Reductive iron mobilization from ferritin is determined by the mineral core reduction and dissolution which is dependent on the electron-relay efficiency of the quinone mediators, in situ-generated ROS and transient intermediates. The $E_{1/2}$ values of the quinone mediators play a primary role in dictating their electron-relay efficiency, where quinones with $E_{1/2}$ values lying not very far, not too close to NADH released higher amounts of iron. Molecular structure is another critical aspect that determines the electron shuttling capability of quinones. Presence of appropriate functional groups in desired positions providing favorable iron-chelation sites and the ability to form intramolecular H-bonding are seen to favor core reduction and higher iron release. Further, the ability of these quinones to inhibit/generate ROS in the reaction medium also influences the iron dissolution/mobilization. Owing to the above mentioned criteria, PM and JG were found to release the maximum amount of iron under both aerobic and anaerobic conditions. The rates of NADH oxidation and dissolved-O_2 consumption kinetic profiles of the chosen mediators were not directly tied to their iron-release kinetic rates. This indicates a complex interplay of a number of other factors beyond their structure–reactivity relationships with $NADH/O_2$, toward deciding the ultimate iron-release kinetics. Thus, the current work would not only helps in understanding the ferritin iron-release mechanism but also can be exploited for understanding iron acquisition/mobilization in plants/microbes. This work can be further extended toward understanding the involvement of quinone mediators in biologic ET reactions (energy transduction) and to control O_2-based cellular metabolism (O_2 activation) and toxicity.

Supplementary Information The online version contains supplementary material available at https://doi.org/10.1007/s00775-024-02058-w.

Acknowledgements This work was supported by Science and Engineering Research Board (SERB), India (CRG/2020/005332) and Science and Technology Department, Odisha, India (ST-SCST-MISC-0036-2023) to R.K.B. We are thankful to Dr. Anil K. Tyagi and Dr. Garima Khare (University of Delhi, South Campus) for their generous support in providing the *Mtb* Bfr clone and Mr. Subrat Kumar Naik for his experimental help.

Data availability The data of the findings of this study will be available on request.

Declarations

Conflict of interest The authors declare no competing financial interests.

References

1. Theil EC, Tosha T, Behera RK (2016) Acc Chem Res 49:784–791
2. Crichton R (2009) Iron metabolism. Wiley, pp 17–58
3. (2007) In: H. B. G. Ivano Bertini, Edward I. Stiefel and Joan S. Valentine (ed). University Science Books, NY
4. Koppenol WH, Hider RH (2019) Free Radical Biol Med 133:3–10
5. Bou-Abdallah F (2010) Biochem Biophys Acta 1800:719–731
6. Sheftel AD, Mason AB, Ponka P (2012) Biochimica Biophysica Acta (BBA) Gen Subj 1820:161–187
7. Frey PA, Reed GH (2012) ACS Chem Biol 7:1477–1481
8. Theil E (1987) Annu Rev Biochem 56:289–315
9. Parida A, Behera RK (2023) Methods Mol Biol 2671:121–134
10. Harrison PM, Arosio P (1996) Biochem Biophys Acta 1275:161–203
11. Chasteen ND, Harrison PM (1999) J Struct Biol 126:182–194
12. Behera RK, Theil EC (2014) Proc Natl Acad Sci USA 111:7925–7930
13. Parida A, Mohanty A, Kansara BT, Behera RK (2020) Inorg Chem 59:629–641
14. Zhao G, Su M, Chasteen ND (2005) J Mol Biol 352:467–477
15. Theil EC and Behera RK (2013) In: Y. W. Takafumi Ueno (ed) Coordination chemistry in protein cages. pp. 1–24
16. Maity B, Fujita K, Ueno T (2015) Curr Opin Chem Biol 25:88–97
17 Taher M, Maity B, Nakane T, Abe S, Ueno T, Mazumdar S (2022) Angew Chem 61:e202116623
18 Honarmand Ebrahimi K, Hagedoorn PL, Hagen WR (2015) Chem rev 115:295–326
19 Mohanty AKM, Jena SS, Behera RK (2021) Biomacromol 22:1389–1398
20. Mohanty A, Parida A, Raut RK, Behera RK (2022) ACS bio & med chem Au 2:258–281
21. Parida A, Mohanty A, Raut RK, Padhy I, Behera RK (2023) Inorg Chem 62:178–191
22. Khare G, Nangpal P, Tyagi AK (2013) Biochemistry 52:1694–1704
23. Stefanini S, Desideri A, Vecchini P, Drakenberg T, Chiancone E (1989) Biochemistry 28:378–382
24. Behera RK, Torres R, Tosha T, Bradley JM, Goulding CW, Theil EC (2015) J Biol Inorganic Chem JBIC Pub Soc Biol Inorg Chem 20:957–969
25. Douglas T, Ripoll DR (1998) Protein Sci 7:1083–1091
26. Chandramouli B, Bernacchioni C, Di Maio D, Turano P, Brancato G (2016) J Biol Chem 291:25617–25628
27. Uchida M, Kang S, Reichhardt C, Harlen K, Douglas T (2010) Biochem Biophys Acta 1800:834–845
28. Bradley JM, Moore GR, Le Brun NE (2017) Curr Opin Chem Biol 37:122–128
29. Kwak Y, Schwartz JK, Haldar S, Behera RK, Tosha T, Theil EC, Solomon EI (2014) Biochemistry 53:473–482
30. Theil EC (2013) Inorg Chem 52:12223–12233
31. Ponka P, Richardson DR (1997) Blood 89:2611–2613
32. La A, Nguyen T, Tran K, Sauble E, Tu D, Gonzalez A, Kidane TZ, Soriano C, Morgan J, Doan M, Tran K, Wang CY, Knutson MD, Linder MC (2018) Metallomics Integr Biometal Sci 10:154–168
33. Sala D, Ciambellotti S, Giachetti A, Turano P, Rosato A (2017) J Chem Inf Model 57:2112–2118
34. Bou-Abdallah F, Paliakkara JJ, Melman G, Melman A (2018) Pharmaceuticals 11:120
35. Dehner C, Morales-Soto N, Behera RK, Shrout J, Theil EC, Maurice PA, Dubois JL (2013) J Biol Inorg Chem JBIC Pub Soc Biol Inorg Chem 18:371–381
36. Mohanty A, Parida A, Subhadarshanee B, Behera N, Subudhi T, Koochana PK, Behera RK (2021) Inorg Chem 60:16937–16952
37 Punchi Hewage AND, Fontenot L, Guidry J, Weldeghiorghis T, Mehta AK, Donnarumma F, Rivera M (2020) Pathogens 9:980
38. Cassat JE, Skaar EP (2013) Cell Host Microbe 13:509–519
39. Chao A, Sieminski PJ, Owens CP, Goulding CW (2019) Chem Rev 119:1193–1220
40. Mohanty A, Subhadarshanee B, Barman P, Mahapatra C, Aishwarya B, Behera RK (2019) Inorg Chem 58:4741–4752
41. Kappler A, Bryce C, Mansor M, Lueder U, Byrne JM, Swanner ED (2021) Nat Rev Microbiol 19:360–374
42. Einsle O (2012) Structure 20:1132–1134
43. Mancias JD, Wang X, Gygi SP, Harper JW, Kimmelman AC (2014) Nature 509:105–109
44. Tosha T, Behera RK, Ng HL, Bhattasali O, Alber T, Theil EC (2012) J Biol Chem 287:13016–13025
45. Koochana PK, Mohanty A, Das S, Subhadarshanee B, Satpati S, Dixit A, Sabat SC, Behera RK (2018) Biochim Biophys Acta 1862:1190–1198
46 Melman G, Bou-Abdallah F, Vane E, Maura P, Arosio P, Melman A (2013) Biochimica Biophysica Acta (BBA) Gen Subj 1830:4669–4674
47. Badu-Boateng C, Naftalin RJ (2019) Free Radical Biol Med 133:75–87
48. Koochana PK, Mohanty A, Subhadarshanee B, Satpati S, Naskar R, Dixit A, Behera RK (2019) Dalton Trans 48:3314–3326
49. Radisky DC, Kaplan J (1998) Biochem J 336(Pt 1):201–205
50. Kidane TZ, Sauble E, Linder MC (2006) Am J Physiol Cell Physiol 291:C445-455
51. Theil EC (2010) Ann N Y Acad Sci 1202:197–204
52. Yao H, Wang Y, Lovell S, Kumar R, Ruvinsky AM, Battaile KP, Vakser IA, Rivera M (2012) J Am Chem Soc 134:13470–13481
53. Yasmin S, Andrews SC, Moore GR, Le Brun NE (2011) J Biol Chem 286:3473–3483
54. Khare G, Nangpal P, Tyagi AK (2017) PLoS One 12:e0169545
55. Koochana PK, Mohanty A, Parida A, Behera N, Behera PM, Dixit A, Behera RK (2021) Journal of biological inorganic chemistry : JBIC : a publication of the Society of Biological. Inorg Chem 26:265–281
56. Saito K, Rutherford AW, Ishikita H (2013) Proc Natl Acad Sci USA 110:954–959
57. Bolton JL, Dunlap T (2017) Chem Res Toxicol 30:13–37
58. Chobot V, Hadacek F (2010) Plant Signal Behav 5:4–8
59. Yurko Y, Elbaz L (2023) J Am Chem Soc 145:2653–2660
60. Huynh MT, Anson CW, Cavell AC, Stahl SS, Hammes-Schiffer S (2016) J Am Chem Soc 138:15903–15910
61 al-Massad FK, Kadir FHA, Moore GR (1992) Biochem J 283:177–180
62. Khare G, Gupta V, Nangpal P, Gupta RK, Sauter NK, Tyagi AK (2011) PLoS One 6:e18570

63. Behera RK, Goyal S, Mazumdar S (2010) J Inorg Biochem 104:1185–1194
64. Quan M, Sanchez D, Wasylkiw MF, Smith DK (2007) J Am Chem Soc 129:12847–12856
65 Ilan YA, Czapski G, Meisel D (1976) Biochimica Biophysica Acta (BBA) Bioenerg 430:209–224
66. Ji X, Liu X, Li M, Shao S, Chang J, Du J, Ma X, Feng X, Zhu L, Yu X, Hu W (2021) J Chem Educ 98:3019–3025
67. Rao PS, Hayon E (1973) J Phys Chem 77:2274–2276
68. Borghese R, Malferrari M, Brucale M, Ortolani L, Franchini M, Rapino S, Borsetti F, Zannoni D (2020) Bioelectrochemistry 133:107456
69. Chrastina A, Welsh J, Rondeau G, Abedinpour P, Borgström P, Baron VT (2020) Chem Med Chem 15:1338–1347
70 Swallow AJ (1982). In: Trumpower BL (ed) Function of quinones in energy conserving systems. Academic Press, pp 59–72
71 Munir S, Shah A, Rauf A, Badshah A, Hussain H, Zia ur R, Ahmad Z (2013) C R Chim 16:1140–1146
72. Jena AB, Samal RR, Kumari K, Pradhan J, Chainy GBN, Subudhi U, Pal S, Dandapat J (2021) Int J Biol Macromol 167:871–880
73. Carmona F, Palacios Ò, Gálvez N, Cuesta R, Atrian S, Capdevila M, Domínguez-Vera JM (2013) Coord Chem Rev 257:2752–2764
74. Muhoberac BB, Vidal R (2019) Front Neurosci 13:1195
75. Theil EC, Behera RK, Tosha T (2013) Coord Chem Rev 257:579–586
76. Rivera M (2023) J Inorg Biochem 247:112306
77. Subramanian V, Evans DG (2012) J Phys Chem B 116:9287–9302
78. Jones T, Spencer R, Walsh C (1978) Biochemistry 17:4011–4017
79 Watt RK, Hilton RJ, Graff DM (2010) Biochimica Biophysica Acta (BBA) Gen Subj 1800:745–759
80. Raymond KN, Allred BE, Sia AK (2015) Acc Chem Res 48:2496–2505
81. Butler A, Theisen RM (2010) Coord Chem Rev 254:288–296
82. Pinho B, Sousa C, Oliveira J, Valentão P, Andrade P (2012) Bioact Compd Types Biol Act Health Eff:181–218
83. Bou-Abdallah F, McNally J, Liu XX, Melman A (2011) Chem Commun 47:731–733
84. Song Y, Buettner GR (2010) Free Radical Biol Med 49:919–962
85 Kumbhar A, Padhye S, Ross D (1996) Biometals Int J Role Metal Ions Biol Biochem Med 9:235–240

Authors and Affiliations

Narmada Behera[1] · Gargee Bhattacharyya[1] · Satyabrat Behera[1] · Rabindra K. Behera[1]

✉ Rabindra K. Behera
beherarabi@nitrkl.ac.in

[1] Department of Chemistry, National Institute of Technology, Rourkela, Odisha 769008, India